

**Georgia Water Resources Institute
Annual Technical Report
FY 2016**

Introduction

MISSION STATEMENT

GWRI strives to improve the science and practice of water resources planning and management in ways that balance quality of life, environmental sustainability, and economic growth. GWRI pursues this mission through its education, research, information dissemination, and technology/knowledge transfer programs at the state, national, and international levels.

Organizational Structure: The GWRI organizational structure includes a Director, Associate Director, Assistant Director, Advisory Board, and technical support staff. The technical support staff comprises several Ph.D. graduate students who work on GWRI projects while carrying out doctoral research, and information technology support staff. The Advisory Board includes representatives from major state and federal water agencies as well as environmental and citizen groups. At Georgia Tech, GWRI reports to the Senior Vice-Provost for Research under the Office of the Provost.

Research Program Sponsorship and Administration: GWRI activities are sponsored by (i) the Department of the Interior/USGS as part of the state and national research programs, and (ii) other national and international funding agencies and organizations supporting research in water related areas. Through its annual state and national competitive programs, GWRI provides research awards to Georgia Universities. The award process includes submission of technical proposals, technical peer reviews, and reviews for relevance to Georgia needs by the State Environmental Protection Division (Georgia EPD).

Other External Funding: In addition to the 104B and 104G programs, GWRI generates additional funding through participation in competitive national and international research programs. Recent funding has been provided by the California Energy Commission, the California Department of Water Resources, NOAA, and the ACF Stakeholders. GWRI involvement in national and international research activities is crucial to maintaining the expert capacity and funding portfolio necessary to provide quality services to the state of Georgia and all other sponsors.

FY2016 RESEARCH PROJECTS THROUGH 104B PROGRAM

- (1) Phosphorus and Metal Speciation Dynamics during Thermal Treatment of Sewage Sludges; Tang, Y.; Georgia Institute of Technology.
- (2) Geostatistical Models for Optimizing Groundwater Monitoring Network in the Lower Apalachicola Chattahoochee Flint (ACF) River basin; Luo, J.; Georgia Institute of Technology.
- (3) Fecal bacteria source tracking, nutrient analysis, and modeling of an urban TMDL watershed; Radcliffe, D. and Habteselassie, M.; University of Georgia.
- (4) Comparison of Oconee and Ocmulgee river basins for sustainable ecosystem and economic development of Middle Georgia; Tollner, E. and Rasmussen, T.; University of Georgia.

OTHER RESEARCH PROJECTS AND ACCOMPLISHMENTS

Climate Change Assessment and Adaptation Planning for River Basins with Estuarine Resources, Aris Georgakakos PI, Georgia Institute of Technology, sponsored by NOAA.

Integrated Forecast and Reservoir Management (INFORM) for Northern California, A.P. Georgakakos PI, Georgia Institute of Technology (Project Partners: Hydrologic Research Center), sponsored by California Department of Water Resources.

RECENT PUBLICATIONS

Dettinger, M., B. Udall, and A.P. Georgakakos, 2015: Western Water and Climate Change. *Ecological Applications*, 25(8), pp. 2069–2093 (Ecol. Soc. of America Centennial Paper).

Sharif, H.E., J. Wang, and A.P. Georgakakos, 2015: Modeling Regional Crop Yield and Irrigation Demand Using SMAP Type of Soil Moisture Data. *Journal of Hydrometeorology*, 16, pp. 904–916. Available at <http://journals.ametsoc.org/doi/pdf/10.1175/JHM-D-14-0034.1>.

Kistenmacher, M., and A.P. Georgakakos, 2015: Assessment of Reservoir System Variable Forecasts, *Water Resources Research*, 51, pp. 3437–3458 (doi:10.1002/2014WR016564).

Chen, C.-J., and A.P. Georgakakos, 2015: Seasonal Prediction of East African Rainfall. *International Journal of Climatology*, 35, pp. 2698–2723 (doi:10.1002/joc.4165).

Georgakakos, A.P., P. Fleming, M. Dettinger, C. Peters-Lidard, T.C. Richmond, K. Reckhow, K. White, and D. Yates: Water Resources Chapter, 2014 National Climate Assessment Draft, <http://ncadac.globalchange.gov>, 2014.

Georgakakos, A.P., H. Yao, and K.P. Georgakakos, “Ensemble streamflow prediction adjustment for upstream water use and regulation”, *Journal of Hydrology*, doi: 10.1016/j.jhydrol.2014.06.044, 2014.

Kim, D.H., and A.P. Georgakakos, “Hydrologic River Routing using Nonlinear Cascaded Reservoirs,” *Water Resources Research*, doi: 10.1002/2014WR015662, 2014.

Chen, C-J., and A.P. Georgakakos, “Seasonal Prediction of East African Rainfall,” *International Journal of Climatology*, doi: 10.1002/joc.4165, 2014. *Climate of the Southeast United States: Variability, Change, Impacts, and Vulnerability*, co-author of Chapter 10, “Impacts of Climate Change and Variability on Water Resources in the Southeast USA,” Island Press, Washington DC, 341p, 2013.

Chen, C-J., and A.P. Georgakakos, “Hydro-Climatic Forecasting Using Sea Surface Temperatures—Methodology and Application for the Southeast U.S.,” *Journal of Climate Dynamics*, doi:10.1007/s00382-013-1908-4, 2013.

RECENT REPORTS

Georgakakos, A.P., and M. Kistenmacher (2015): Water Management Scenario Assessments for the ACF River Basin. Technical Report, Georgia Water Resources Institute, Georgia Institute of Technology, Atlanta, Georgia, 41p.

Georgakakos, A.P., and M. Kistenmacher (2015): Value of Drought Prediction for the Management of the ACF River Basin. Technical Report, Georgia Water Resources Institute, Georgia Institute of Technology, Atlanta, Georgia, 34p.

Georgakakos, A.P., and M. Kistenmacher (2012): Unimpaired Flow Assessment for the Apalachicola Chattahoochee-Flint River Basin. Technical Report, Georgia Water Resources Institute, Georgia Institute of Technology, Atlanta, Georgia, 211p.

RECENT CONFERENCE PRESENTATIONS

Georgakakos, A.P., “Integrated Water, Energy, and Environmental Planning in the Rufiji River and Lake Rukwa Basins, Tanzania”, 2016 AGU Fall Meeting, San Francisco, December 15, 2016.

Dettinger, M., B.H. Udall, A.P. Georgakakos, “Western Water and Climate Change--An Overview”, 2016 AGU Fall Meeting, San Francisco, December 12, 2016.

Kistenmacher, M. and A.P. Georgakakos, “Value of Adaptive Drought Forecasting and Management for the ACF River Basin in the Southeast U.S”, 2016 AGU Fall Meeting (Poster), San Francisco, December 13, 2016.

DiVittorio, C. and A.P. Georgakakos, “A Satellite Based Method for Wetland Inundation Mapping”, 2016 AGU Fall Meeting, San Francisco, December 15, 2016.

Kistenmacher, M., and A.P. Georgakakos, “Development of a sustainable water management plan for the ACF River Basin”, 2016 UCOWR/NIWR Annual Water Resources Conference, Pensacola Beach, June 21-23, 2016.

Kistenmacher, M., and A.P. Georgakakos, “Value of adaptive drought management for the ACF river basin”, 2016 UCOWR/NIWR Annual Water Resources Conference, Pensacola Beach, June 21-23, 2016.

Research Program Introduction

Four research projects were funded through the 104B Program (each at \$18,000) in FY2016:

- (1) Phosphorus and Metal Speciation Dynamics during Thermal Treatment of Sewage Sludges; Tang, Y.; Georgia Institute of Technology.
- (2) Geostatistical Models for Optimizing Groundwater Monitoring Network in the Lower Apalachicola Chattahoochee Flint (ACF) River basin; Luo, J.; Georgia Institute of Technology.
- (3) Fecal bacteria source tracking, nutrient analysis, and modeling of an urban TMDL watershed; Radcliffe, D. and Habteselassie, M.; University of Georgia.
- (4) Comparison of Oconee and Ocmulgee river basins for sustainable ecosystem and economic development of Middle Georgia; Tollner, E. and Rasmussen, T.; University of Georgia.

The Georgia Water Resources Institute asked for and received permission to extend the deadline of project (3) into FY2016 to allow the PIs to make field measurements that could not have been completed by the original project deadline.

Phosphorus and Metal Speciation Dynamics during Thermal Treatment of Sewage Sludges

Basic Information

Title:	Phosphorus and Metal Speciation Dynamics during Thermal Treatment of Sewage Sludges
Project Number:	2016GA364B
Start Date:	3/1/2016
End Date:	2/28/2017
Funding Source:	104B
Congressional District:	United States: 5th
Research Category:	Engineering
Focus Category:	Nutrients, Wastewater, Geochemical Processes
Descriptors:	None
Principal Investigators:	Yuanzhi Tang

Publications

There are no publications.

Georgia Water Resources Institute Project 2016 Annual Report

Phosphorus and Metal Speciation Dynamics during Thermal Treatment of Sewage Sludges

PI: Yuanzhi Tang
School of Earth and Atmospheric Sciences
Georgia Institute of Technology
Atlanta, GA 30332-0340

1. Research Background and Objectives

Tremendous amounts of sewage sludges are being produced as the byproducts of wastewater treatment processes, bringing a daunting task for the water industry. In addition to the intrinsic high water content and large volume, sludges often contain a wide range of organic and inorganic contaminants, such as heavy metals, pesticides, herbicides, microorganisms, and pharmaceuticals and personal care products (PPCPs). On the other hand, sludge also consists of a wide range of nutrients and valuable metals at relatively high concentrations, and is increasingly recognized and treated as a resource for the recycling of critical nutrients such as phosphorus (P). In fact, a significant portion of P consumed by human activities is ultimately converged into wastewater treatment plants, making the sludges a great resource for P recycling and reclamation.

In recent years, thermal (e.g. pyrolysis) and hydrothermal treatments (e.g. hydrothermal carbonization; HTC) of sewage sludge have emerged as sustainable treatment techniques, because they can significantly decompose organic pollutants, reduce waste volume, and generate valuable by-products (e.g. chars). During the production of chars, nutrients such as P mostly remain in the solid phase, making it a char-P composite with many potential applications, e.g. P recycling using acid extraction. (Bio)chars produced from thermal treatments have also been recognized as good soil amendments to adjust soil physical and chemical properties and improve soil qualities. With the significant decomposition of organic contaminants during thermal treatment processes, direct soil application of such char-P composite might also be an excellent alternative P recycling and fertilization practice with all the added benefits from chars.

It is well known that the speciation of an element determines its mobility, transport, fate, and bioavailability. Thus, one critical knowledge gap for the abovementioned or any other P recycling/reclamation approaches from thermal treatment derived sludge products is the evolution of P and metal speciation during the thermal treatments, as this relates to the selection of further P recycling techniques as well as the toxicity and bioavailability of metals.

The overall goal of this project is to systematically characterized the speciation of P and metals (Cu and Zn) in raw sludges as well as the pyro- and hydrochars derived from pyrolysis and hydrothermal carbonization treatments of the sludges under varied treatment conditions.

2. Research Approach

2.1. Materials and treatments

Two types of sewage sludges (activated sludge and anaerobic sludge) were collected from F. Wayne Hill Water Resources Center (Gwinnett County, Atlanta, Georgia). The activated sludge represents sludge in its most unprocessed form, while the anaerobic sludge represents sludge that has experienced common processing (e.g. mixing of sludges from different units, dewatering, and anaerobic digestion) and has relatively higher metal contents than the activated sludge. Pyrolysis and HTC were conducted on both the activated and anaerobic sludges. Pyrolysis was conducted in

a tube furnace under N_2 flow (~ 1 mL/sec) at a range of temperatures (250 to 600 °C), with a heating and cooling rate of 200 °C/h and a soaking duration of 4 h. For each treatment condition, 1.0 g of freeze-dried activated sludge was added into a crucible and inserted into the glass tube. All samples were processed in duplicates. The produced solid chars are hereafter referred to as pyrochar. For HTC treatment, wet sludge equivalent to ~ 1.8 g dry mass was weighted into a 20 mL Teflon lined stainless steel hydrothermal reactor. Deionized water was then added to achieve a total weight of 12 g. The reactor was sealed and heated in an oven at 225 °C for 4 or 16 h, then allowed to naturally cool down to 50 °C in an oven. The produced solids (hereafter referred to as hydrochar) and the processed water were separated by centrifugation, and the hydrochar was freeze-dried. The total mass recovery, processed water volume, and dried hydrochar mass were recorded.

2.2. Sequential extraction

Sequential extraction of P in the raw sludges and their derived chars were conducted following the Hedley's method^[1]. Specifically, 150 mg raw sludge or char was added to a 50 mL polypropylene centrifuge tube and sequentially extracted by 20 mL extraction solutions. The reaction tubes were constantly agitated by end-to-end shaking. The samples were first extracted with deionized water for 8 h, followed by 0.5 M $NaHCO_3$, 0.1 M $NaOH$, and 1.0 M HCl solutions, each lasting 16 h. Replicate set of experiments were conducted. At the end of each extraction step, one set of reaction was sacrificially taken down, and the solid and aqueous phases separated by filtration (0.45 μm). The solid residue was freeze-dried for P content and X-ray absorption near edge structure (XANES) analysis, and the filtrate analyzed for P content.

Sequential extraction of Zn and Cu in the raw sludges and their thermal derived chars followed the three-step BCR procedure.^[2] Briefly, 250 mg of dried solids were weighted into 50 mL polypropylene centrifuge tubes, and sequentially extracted with the following steps: (1) soluble/exchangeable fraction: 20 mL acetic acid (0.11 M) for 16 h, (2) reducible fraction 20 mL hydroxylamine hydrochloride (0.1 M, pH 2.0) for 16 h, and (3) oxidizable fraction: 4 mL H_2O_2 (30%), air dried, then 20 mL ammonium acetate (1 M, pH 2.0). The extracted liquids were mixed with certain amount of scandium solution (served as internal standard) and digested by a mixture of concentrated H_2O_2 and HNO_3 (v/v = 1:1) on a heating plate (100 °C), then diluted for final analysis. The untreated solids and extracted solid residues were ashed in an oven at 550 °C, followed by digestion with aqua regia and further dilution for concentration analysis. Metal contents in the extracted liquid, solid residues, and the untreated solids were determined by ICP-MS. The extractions were conducted in triplicates.

2.3. X-ray absorption spectroscopy (XAS) analysis

P K-edge X-ray absorption near edge spectroscopy (XANES) data were collected at Beamline 14-3 at the Stanford Synchrotron Radiation Lightsource (SSRL), Menlo Park, CA. The raw sludges and their derived chars were ground into fine powders and brushed evenly onto P-free Kapton tapes. Excess powders were blown off to achieve a homogeneous and thin film. The sample chamber was maintained under He atmosphere at room temperature, and XANES data were collected in fluorescence mode using a PIPS detector. Energy calibration used $AlPO_4$ by setting the edge position (peak maxima of the first derivative) to be 2152.8 eV. XANES spectra were collected at 2100–2485 eV. Multiple scans were collected for each sample and averaged for further analysis. Reference compounds included: (1) $FePO_4 \cdot 2H_2O$ and phosphate sorption on ferrihydrite, representing Fe-associated P; (2) $AlPO_4$ and phosphate sorption on γ -alumina, representing Al-

associated P; (3) octacalcium phosphate and hydroxylapatite, representing Ca-associated P; (4) phytic acid, representing P associated with organic functional groups.

Cu and Zn K-edge XAS analysis of sludge samples and reference compounds were collected at Beamlines 5-BM-D and 12-BM-B at Advanced Photo Source (APS; Argonne National Laboratory, Lemont, IL), as well as Beamline 4-1 at SSRL. Energy calibration used the corresponding metal foils. Freeze dried raw sludges, pyrochars, or oven dried hydrochars were ground into fine powders and packed into a Teflon sample holder covered with Kapton tape. Both XANES and extended X-ray absorption fine structure (EXAFS) data were collected in fluorescence mode at room temperature. XAS data were also collected on a range of reference compounds. Cu reference compounds include Cu(I) and Cu(II) sulfides (Cu_2S and CuS), Cu-Fe-sulfides (chalcopyrite CuFeS_2 and cubanite CuFe_2S_3), and Cu-humic complex. Zn reference compounds include Zn-cysteine complex, pure ZnS , two ZnS polymorphs with Fe impurity (sphalerite and wurtzite), Zn-doped ferrihydrite, and hopeite [$\text{Zn}_3(\text{PO}_4)_2 \cdot 4\text{H}_2\text{O}$].

XAS data processing and analysis used the softwares SIXpack and Ifeffit. Multiple scans were energy calibrated and averaged for further analysis. Principal component analysis (PCA) was conducted to determine the number of components needed for obtaining reasonable fits. Using the corresponding reference compound spectra library, target transformation was conducted to determine appropriate candidate compounds. Linear combination fitting (LCF) was conducted on XANES and/or EXAFS regions.

Table 1. Pyrolysis and HTC treatment conditions, sample label, and solid characteristics of the sludges.

Sludge type	Treatment	Condition	Sample label	Solid recovery (%)	Solid P content (%)	P recovery (%)
Activated sludge	Raw	Freeze dried	Sludge	N/A	4.1±0.1	N/A
	Pyrolysis	250 °C, 4 h	S250	69.1±5.5	5.7±0.1	95.8
	Pyrolysis	450 °C, 4 h	S450	45.6±1.1	8.9±0.1	98.2
	HTC	225 °C, 4h	SHTC4h	55.2±4.1	7.6±0.1	101.3
	HTC	225 °C, 16h	SHTC16h	48.5±0.9	8.1±0.1	89.3
Anaerobically digested sludge	Raw	Freeze dried	Ana	N/A	3.3±0.1	N/A
	Pyrolysis	250 °C, 4 h	A250	72.2±4.2	4.7±0.1	103.1
	Pyrolysis	450 °C, 4 h	A450	47.2±6.0	7.2±0.2	103.2
	HTC	225 °C, 4h	AHTC4h	55.6±5.0	4.9±0.1	81.7
	HTC	225 °C, 16h	AHTC16h	49.8±4.5	6.1±0.1	95.5

3. Research Outcome: P speciation

3.1. P speciation in raw sludges

Overall characteristics of the raw sludges and their derived chars, (hydro)thermal treatment parameters, and sample labels are presented in Table 1. In general, the physicochemical properties (e.g., elemental composition, physical states, and stability) of sewage sludges are dependent on many factors, such as sludge source, treatment techniques at the waste water treatment plant, as well as sludge collection and processing steps. Activated sludge directly from the biological treatment unit generally consists of active granules (e.g. microbial cells and other organic/inorganic components) and P can present in different forms (in terms of both molecular entity and complexation form) and distribute heterogeneously, depending on the treatment techniques. Anaerobic sludge receives both activated sludge and sludges from other units, and could have experienced extensive mechanical and thermal dewatering/drying and digestion processes. LCF of P XANES spectra showed significant difference of P speciation between the

activated and anaerobic sludges (Figure 1 and 2). If only considering species with > 5% abundance, phytic acid (42%), AlPO_4 (34%), and alumina-adsorbed phosphate (15%) are the three main species identified in the activated sludge, while AlPO_4 (40%), phytic acid (20%), ferrihydrite-adsorbed phosphate (13%), octacalcium phosphate (OctaCa; 16%), and alumina-adsorbed phosphate (11%) were the main species identified in the anaerobic sludge. The P XANES results showed overall less organic P and more Fe/Ca-associated P species in the anaerobic sludge than activated sludge. This is most likely resulted from: 1) the release of intracellular or cell-bound P during the processing of activated sludge, which subsequently interacted with metals such as Fe and Ca, 2) higher metal contents in anaerobic sludge than in activated sludge.

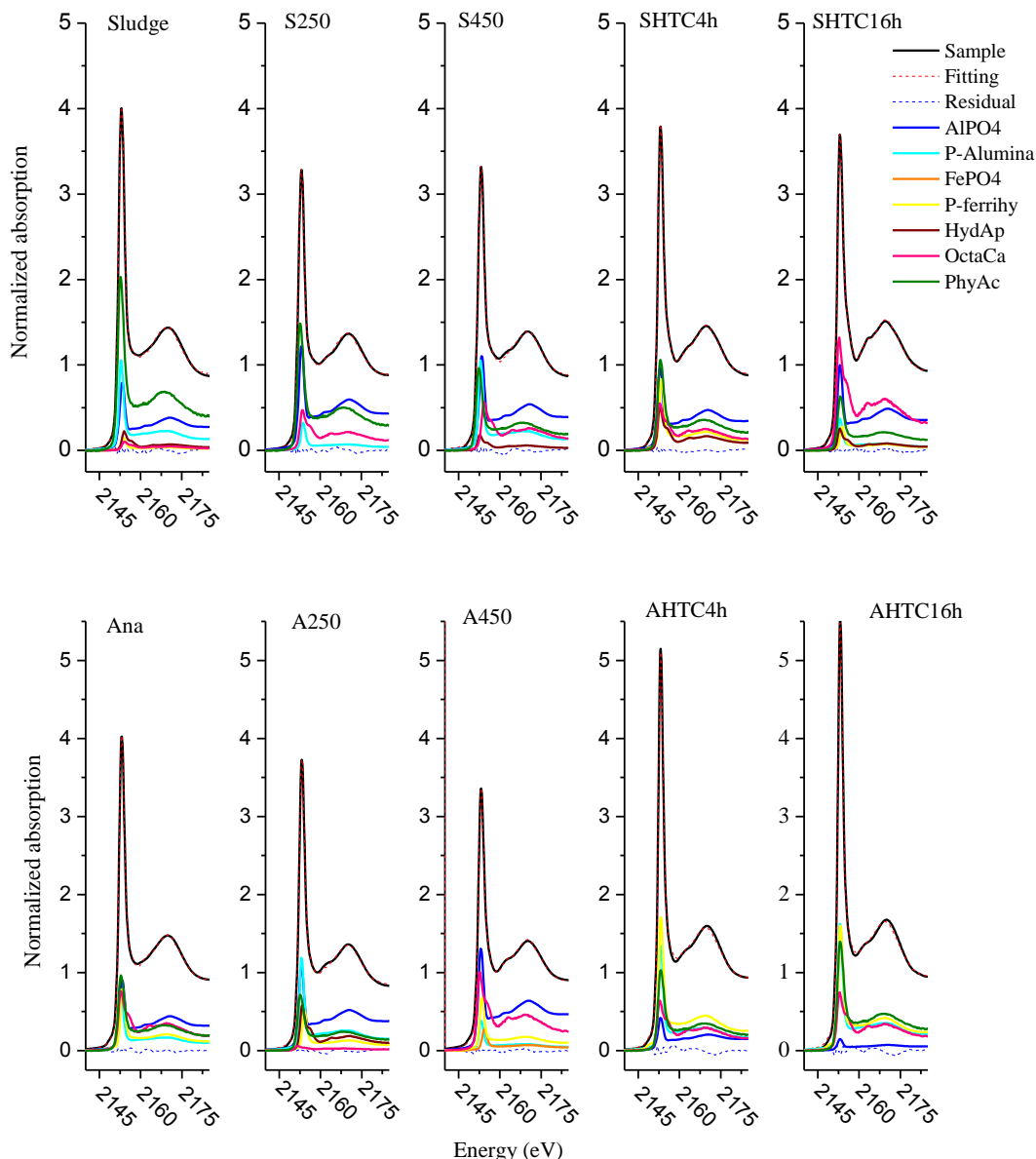


Figure 1. Linear combination fittings of P XANES spectra of activated sludge, anaerobic sludge, and their pyrochars and hydrochars. Fitted components include AlPO_4 , phosphate sorption on γ -alumina (P-Alumina), FePO_4 , phosphate sorption on ferrihydrite (P-ferrihy), hydroxyapatite (HydAp), octacalcium phosphate (OctaCa), and phytic acid (PhyAc).

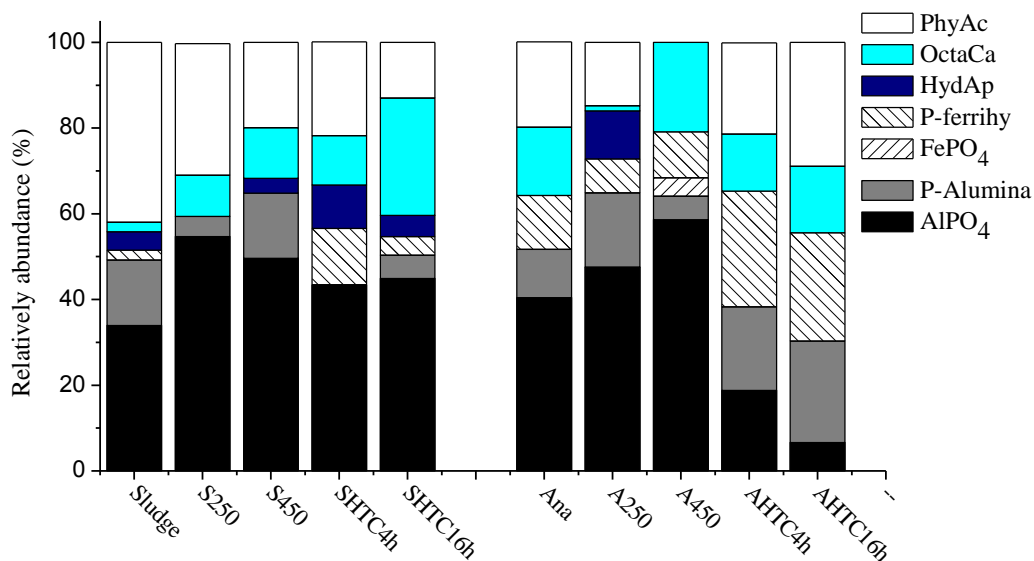


Figure 2. Relative abundance of different P species in activated sludge (Sludge), anaerobically digested sludge (Ana), and their derived pyrochars and hydrochars, as quantified by linear combination fitting of their P XANES spectra.

3.2. P speciation changes during pyrolysis

After the pyrolysis of activated sludge, the most significant changes based on P XANES LCF results are the decrease of phytic acid (42%, 30%, and 20% for raw sludge, S250, and S450, respectively), as well as the increase of Al- and Ca-associated P (Figure 1 and 2). Al-associate P included contributions from both AlPO_4 and phosphate sorption on alumina. Ca-associated P included contributions from both OctaCa and hydroxylapatite (HydAP). The relative abundance of OctaCa (and total Ca-associated P) increased from ~2% (6.5%) for raw sludge to 9.6% (9.6%) and 12% (15.3%) for S250 and S450 pyrochars, respectively. The relative abundance of AlPO_4 (and total Al associated P) increased from 34% (49%) to 55% (59%) and 50% (65%) for sludge, S250, and S450, respectively.

After the pyrolysis of anaerobic sludge, the relative abundance of phytic acid also significantly decreased to 15% (sample A250) and 0% (sample A450), as compared to 20% in the raw anaerobic sludge (sample Ana). The relative abundance of Ca- and Al-associated P also increased after pyrolysis, although not monotonically. The relative abundance of OctaCa (and total Ca-associated P) was 16% (16%), 1.2% (12.4%), and 21% (21%) for Ana, A250, and A450, respectively. The relative abundance of AlPO_4 (and total Al-associated P) increased from 40% (52%) in the raw anaerobic sludge (Ana) to 48% (65%) and 59% (65%) for A250 and A450, respectively. Pyrolysis seemed to have little effects on the relative abundance of Fe-associated P.

Overall, these results suggested that pyrolysis can significantly alter the complexation states of P, and the effects were dependent on pyrolysis temperature and feedstock characteristics (e.g. initial P speciation and metal composition). The decrease of phytic acid (or organics bound P) and increase of metal complexed P (mainly with Ca and Al) are most likely caused by two processes during pyrolysis: 1) the stripping of organic functional groups from the phosphate moiety and the subsequent complexation of phosphate with metals, which appeared to be more significant at higher temperature, and 2) in the case of activated sludge, the breakdown of

polyphosphate into shorter chained polyphosphate, pyrophosphate, and orthophosphate that created additional P-O bonds available for metal complexation.

3.3. P speciation changes during hydrothermal carbonization

Our previous work demonstrated that the main P entity in hydrochars from HTC treatment was orthophosphate, regardless of the feedstock type (activated sludge vs. anaerobic sludge) [3]. Therefore, for HTC treatment, we only need to focus on examining the complexation states of orthophosphate after HTC treatment.

Based on P XANES LCF results, HTC significantly altered the P speciation in both activated and anaerobic sludges, with similarities and differences discussed below (Figure 1 and 2). For activated sludge, the relative abundance of Fe-associated P (all as ferrihydrite adsorbed phosphate) increased after HTC, from 2.3% in raw activated sludge to 13% and 4.4% in its HTC4h and HTC16h hydrochars, respectively. Similar to the effects of pyrolysis, the relative abundance of phytic acid decreased, from 42% in raw sludge to 22% and 13% in SHTC4h and SHTC16h, respectively. The relative abundance of Ca-associated P also increased, with the abundance of OctaCa (and total Ca-associated P) increasing from 2.2% (6.6%) for raw sludge to 11.5% (21.6%) and 27% (32%) for SHTC4h and SHTC16h, respectively. In contrast to the increase of total Al-associated P (and AlPO_4) after pyrolysis, the abundance of total Al-associated P remained unchanged after HTC (49%, 43%, and 50% for raw sludge, SHTC4h, and SHTC16h, respectively), although there were slight increases in AlPO_4 (34%, 43%, and 45% for raw sludge, respectively).

For anaerobic sludge, all the Fe-associated P existed as ferrihydrite adsorbed phosphate, and their relative abundance increased after HTC from 13% for raw anaerobic sludge (sample Ana) to 27 and 25% for AHTC4h and AHTC16h, respectively. The abundance of total Al-associated P (and AlPO_4) decreased from 52% (40%) for Ana to 38% (19%) and 30% (7%) for AHTC4h and AHTC16h, respectively, while that of alumina adsorbed P increased from 11% for Ana to 20% and 24%, for AHTC4h and AHTC16h, respectively. Contrary to that of activated sludge and the effects of pyrolysis, there was a slightly increase in the relative abundance of phytic acid in the hydrochars of anaerobic sludge (21% and 29% for AHTC4h and AHTC16h, respectively, compared to 20% for Ana). The relative abundance of OctaCa remained constant (13% and 16% for AHTC4h and AHTC16h, respectively, compared to 16% for Ana).

The P speciation changes during HTC may be collectively controlled by the composition and states of metals with high affinity to phosphate and the thermochemical reactions occurred during HTC. First of all, reactions occurred during HTC may homogenize phosphates and expose them to various metals and minerals, especially for activated sludge. During HTC, reactions such as hydrolysis, decarboxylation, and polymerization were found to be involved in the transformation of biomass. These reactions were responsible for the hydrolysis of polyphosphate into orthophosphate for activated sludge and exposed the intracellular and organic-bound P to metals such as Ca and Fe, to certain extent similar to the effects of anaerobic digestion. This explains the decrease of phytic acid and increasing abundance of Ca- and Fe-associated P after HTC of activated sludge, as well as their similarity to P speciation in Ana. For HTC of anaerobic sludge, since P in the raw sludge has been relatively homogenized, the magnitude of alterations was much smaller than that for activated sludge (more changes in Fe- and Al-associated P). Secondly, metals such as Fe, Ca, and Al have higher affinity to phosphate than metals such as Na, K, and Mg, and are more abundant than metals such as Cu and Zn, thus phosphate are more likely associated with them. Moreover, the relative abundance and forms of these metals determine the P association stoichiometry and capacity (e.g., Fe mostly present as hydroxide minerals and bound

P as surface adsorbed form, while Ca formed Ca-phosphate minerals in competition with its carbonate and sulfate mineral phases). Since there was a much higher Fe content in anaerobic sludge (~9%) than in activated sludge (~3.6%), higher Fe association with P was found in anaerobic sludge and its hydrochars.

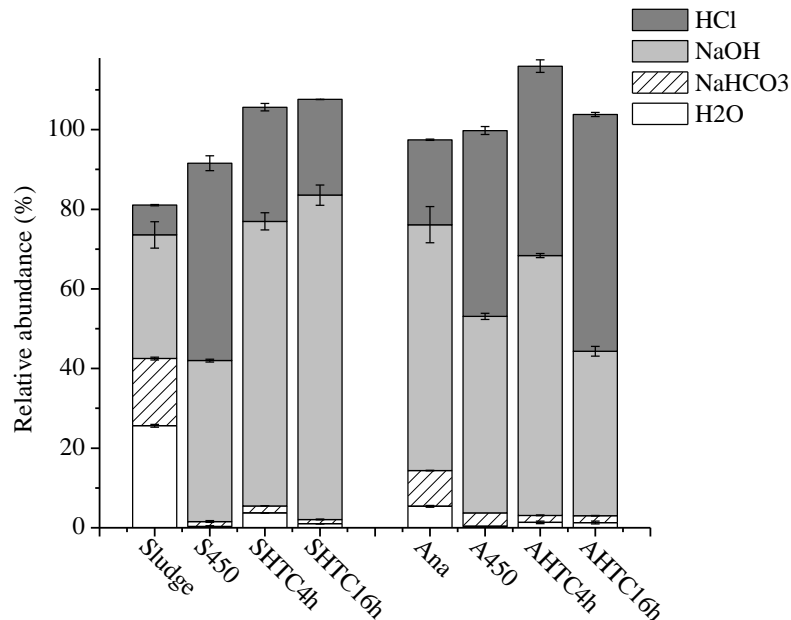


Figure 3. Distribution of P in sequential extracts of sludges and their derived pyrochars and hydrochars. Total sums did not equal to 100%, due to the remaining P in the residue and analytical errors.

3.4. Chemical fractionation by sequential extraction

Sequential extraction showed different P fractionation behaviors between the two sludges and after their pyrolysis and HTC treatments (Figure 3). For activated sludge, a significant amount of P partitioned in the H₂O (26%) and NaHCO₃ (17%) fractions, and these two fractions became negligible after pyrolysis and HTC processing (<2%). After pyrolysis at 450 °C, the NaOH and HCl fractions increased respectively to 40% and 49%, compared to 31% and 7% for raw sludge, respectively. Although HTC increased P partitioning in both NaOH and HCl fractions, the enhancement was more significant for the NaOH fraction (~71% and 81% for SHTC4h and SHTC16h, respectively) than for the HCl fraction (~28% and 24% for SHTC4h and SHTC16h, respectively). For anaerobic sludge, the relatively mobile H₂O (6%) and NaHCO₃ (8%) fractions were much smaller compared to those of activated sludge, and both decreased significantly after pyrolysis and HTC treatment. After pyrolysis at 450 °C, the NaOH fraction decreased from 62% to 49% and the HCl fraction increased from 21% to 47%. The significant enhancement in the HCl fraction also similarly occurred during the pyrolysis of activated sludge. HTC did not significantly increase the NaOH fraction in the hydrochars of anaerobic sludge (65% and 41% for AHTC4h and AHTC16h, respectively, compared to 62% for the raw anaerobic sludge). However, HTC greatly enhanced the HCl fraction (47% and 57% for AHTC4h and AHTC16h, respectively, compared to 21% for the raw anaerobic sludge).

These results suggested that both pyrolysis and HTC substantially stabilized P during the treatment processes, with the stabilization mechanism being different and feedstock-dependent. To further elucidate the stabilization mechanism and the chemical nature of acid/base partitioning

of different P species, we conducted P XANES and LCF analysis on the solid residues after each extraction step (Figure 4). The obtained P speciation information was also compared to the speciation fractions assuming no loss during extraction to evaluate the relative extraction extent of each P species.

During H₂O extraction, AlPO₄ was the main P species being preferentially extracted for activated sludge, if neglecting the small contribution from ferrihydrite adsorbed P and HydAP (2.3% and 4.3%, respectively). AlPO₄, alumina adsorbed phosphate, and OctaCa were all preferentially extracted for anaerobic sludge. During NaHCO₃ extraction, AlPO₄, OctaCa, and phytic acid were the main P species preferentially extracted from activated sludge. OctaCa and phytic acid were the main species extracted from anaerobic sludge. Since H₂O and NaHCO₃ did not extract significant amounts of P from the pyrochars and hydrochars, data of the solid residues were not presented. AlPO₄, alumina adsorbed P, ferrihydrite adsorbed P, and phytic acid were extracted during NaOH extraction of the two raw sludges.

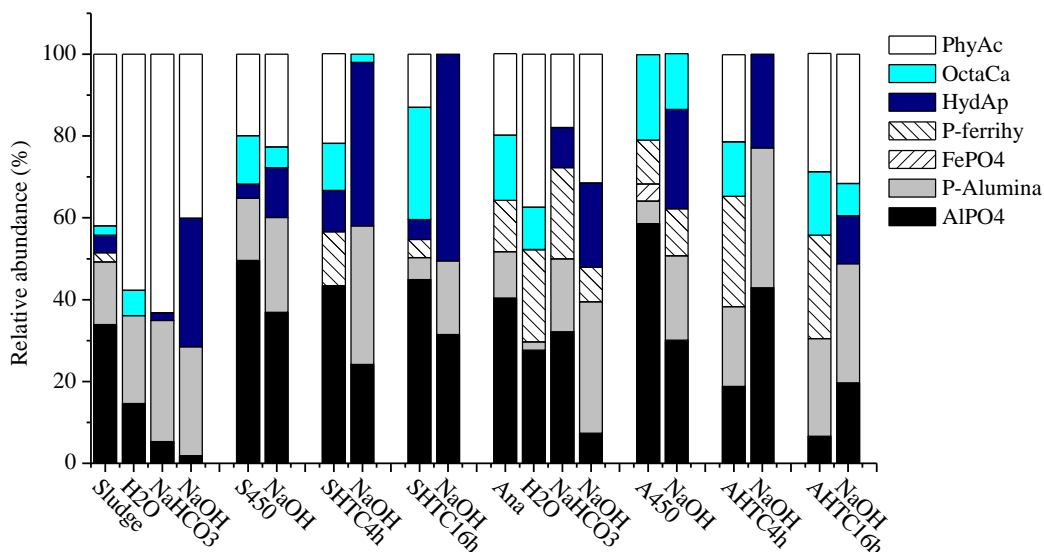


Figure 4. Relative abundance of different P species in sludges and their chars, as well as the solid residuals after each sequential extraction step of the sludges and chars, as quantified by linear combination fitting of their P XANES spectra.

For the char samples (i.e. pyrochars from pyrolysis and hydrochars from HTC), the changes following H₂O-NaHCO₃-NaOH extraction were not always consistent for all the samples. For all the char samples produced by pyrolysis and HTC, the relative abundance of ferrihydrite adsorbed PO₄ significantly decreased or completely disappeared after NaOH extraction, especially for the hydrochar samples (Figure 4). AlPO₄ (except for AHTC16h), OctaCa, and phytic acid were all extracted during NaOH extraction for all the char samples, with varied degrees of extraction. Although the alumina adsorbed P species in the hydrochar of anaerobic sludge was extracted by NaOH, that in all pyrochars and hydrochars of activated sludge was not extracted (or even enhanced). Compared to the raw sludges, whose AlPO₄, alumina adsorbed phosphate, OctaCa, and phytic acid could be extracted to different degrees by H₂O or NaHCO₃, these species in the chars were relatively more stabilized and can only be extracted by NaOH or HCl, suggesting that physical constraints (e.g. embedment of P species into the char structure) may also play a role in P stabilization.

In general, ferrihydrite-adsorbed P and Al-associated P was preferentially extracted during the NaOH step, which was chemically sound and consistent with previous results for soil samples [4]. Phytic acid was also mostly extracted only during the NaOH step. Ca-associated P remained throughout the H₂O-NaHCO₃-NaOH steps, which was also chemically sound and consistent with the general low solubility of Ca-P minerals (e.g. apatite). One interesting observation was that, although HydAP was not identified (or only constituted a very small fraction) in the raw sludge and char samples, it was present abundantly and disproportionately in the residues after NaOH extraction. Amorphous and more crystalline Ca phosphates differ in the relative intensity of the post-edge shoulder and second peak [5], thus it was possible that OctaCa (and less crystalline Ca phosphate) transformed into HydAP during the sequential extraction process. This was also in agreement with the fact that HydAP is more stable than OctaCa, and only dissolves in HCl, instead of NaOH.

4. Research Outcome: Metal Speciation

4.1. Cu and Zn speciation in raw sludges

Cu exists predominantly as sulfide phases with a small amount of organic complex (fitted as Cu-humic complex). The two sludges differ mainly in the relative abundance of Cu₂S and CuS (activated sludge consists of more Cu₂S than CuS, while anaerobically digested sludge is the opposite), and have similar abundance of the Cu-Fe-sulfide phase cubanite (~30%). The abundance of organic complex (Cu-humic) in both samples was similarly low (<11% in both sludges). Regarding the speciation of Zn, characteristic differences between the two raw sludges were observable. Similar to Cu, a significant fraction of Zn existed as sulfide minerals (~40% in activated sludge and ~80% in anaerobic sludge). In addition to sulfide minerals, Zn-phosphate phases (fitted as hopeite) and Zn-associated with Fe oxides (fitted as Zn-doped ferrihydrite) were also present in the raw sludges. These two species similarly accounted for ~30% in activated sludge, while present in less amount in anaerobic sludge (<15%).

Regarding the difference between activated sludge and anaerobic sludge, little alteration occurred for Cu after anaerobic digestion, since most of the Cu already exists as (relatively stable and barely soluble) sulfide phases in activated sludge. For Zn, however, there are more sulfides and less Zn-phosphate and Zn-doped ferrihydrite in anaerobic sludge than in activated sludge, possibly due to P utilization and Fe reduction by microbes and subsequent dissolution and transformation of these phases under anaerobic condition. However, without systematic tracking of the flow and speciation of these elements during sewage collection and wastewater treatment processes, it is challenging to reveal the exact mechanisms controlling the relative abundance of difference species in these sludges.

Sequential extraction results showed that in both activated and anaerobic sludges, Cu similarly presents mostly in the oxidizable fraction (~50%), followed by the residual fraction (20-30%) and reducible fraction (~15%). This is consistent with LCF results of XAS showing that sulfides and Cu-HA complex are the main Cu species. Compared to Cu, Zn partitions mostly in the soluble/exchangeable and reducible fractions (~35% each), and less in the oxidizable fraction and the residual fraction is negligible.

4.2. Effects of pyrolysis on Cu and Zn speciation

Pyrolysis significantly modified Cu and Zn speciation, as can be determined from Cu and Zn XANES and EXAFS analysis. Two main features in the Cu XANES spectra distinguish the raw activated sludge and its pyrochars: the intensity at ~8986 eV decreased and intensity at 8998

eV increased after pyrolysis. The magnitude of change increased as pyrolysis temperature increased. For Cu speciation, pyrochars from activated sludge seem to have experienced the most significant changes, with increasing fraction of Cu-organic complex (e.g. Cu-HA) and decreasing fraction of Fe sulfide species after pyrolysis. The changes during pyrolysis of anaerobic sludge are less significant, only with changes in the relative abundance of different sulfide phases. Regarding Zn speciation, the primary change is the decrease of Zn sulfide and the increase of Zn-doped ferrihydrite after pyrolysis. After pyrolysis, the abundance of wurtzite in both sludges significantly decreased (from ~40% to ~10% and ~80% to ~40%, for activated and anaerobically digested sludges, respectively). Zn-doped ferrihydrite increased to ~50%, compared to ~30% in the raw activated sludge. It was likely that the Zn sulfide phases transformed into Zn-doped ferrihydrite under the pyrolysis conditions. Spectromicroscopy analysis showed that the sizes of Cu and Zn hot spots did not change after pyrolysis, while the speciation change was consistent with the bulk speciation evolution. Pyrolysis was shown to significantly alter the mobility of Cu and Zn, in terms of their partition in sequential extracts. After pyrolysis, Cu in all three extractable fractions significantly decreased and migrated into the residual fraction (~80%), and the change was more significant at higher pyrolysis temperature. Similar to Cu, the partition of Zn in the soluble/exchangeable fraction is also reduced (from ~35% to ~10%) and the residual fraction slightly increased. The oxidizable fraction increased significantly, from ~10% in raw sludges to ~35 to 60% in the pyrochars (as compared to decrease of this fraction for Cu).

4.3. Effects of HTC on Cu and Zn speciation

Despite the difference in initial composition and complex reactions under hydrothermal conditions, Cu XAS spectra of hydrochars from different feedstocks and treatment temperatures are very similar and significantly different from those of pyrochars. LCA results showed the dominance of cubanite and chalcopyrite in the hydrochars, with an abundance of more than 80%, compared to less than 40% in the raw sludges. No CuS or Cu₂S were identified in the hydrochars. Both cubanite and chalcopyrite are important Cu minerals that typically form under hydrothermal conditions and intergrowth of these two minerals was commonly found. Considering the presence of abundant Fe and S in the samples and the nature of hydrothermal conditions, the formation of these minerals during HTC treatment is chemically sound. Regarding the effects of HTC on Zn, the changes following HTC are less significant than those for Cu. The most significant changes are observed for HTC of anaerobic sludge at 225 °C, with the abundance of Zn sulfides (wurtzite) increased from ~80% in the raw sludge to ~95% in the char.

Following HTC treatment, the soluble/exchangeable and reducible Cu fractions became negligible (< 3% and 6%, respectively), and the residual fraction was greatly enhanced, similar to the effect of pyrolysis. Although the absolute metal content in the oxidizable fraction remained mostly unchanged, the relative abundance actually decreased following HTC (from ~50% in feedstock to ~30 to 40% in hydrochars). The effect was similar for both activated and anaerobic sludge. XAS fitting showed Cu exists predominantly as Cu-Fe-sulfide, obviously it partitions into both the oxidizable and residual fractions. The transformation of pure sulfides to Cu-Fe-sulfides is possibly responsible for the stabilization (with Zn-Fe-sulfide being more difficult to be oxidized). Regarding Zn, the soluble/exchangeable and reducible fractions decreased and the oxidizable fraction increased after HTC treatment. The residual fraction also increased, and was more significant for hydrochars of activated sludge than those of anaerobic sludge.

In summary, HTC also stabilizes heavy metals in the sewage sludge, although not as effective as that of pyrolysis treatment.

5. Research Products

Peer reviewed journal articles

- Rixiang Huang, Yuanzhi Tang. Evolution of phosphorus complexation and mineralogy during (hydro)thermal treatments of activated and anaerobically digested sludge: Insights from sequential fractionation and P K-edge XANES. *Water Research*. 2016, 439-447.
- Rixiang Huang, Bei Zhang, Emily Saad, Yuanzhi Tang. Evolution of heavy metal speciation during (hydro)thermal treatments of sewage sludges. *Environmental Science & Technology*. In revision.
- Rixiang Huang, Ci Fang, Xiaowei Lu, Rongfeng Jiang, Yuanzhi Tang. Transformation of phosphorus during (hydro)thermal treatments of solid biowastes: Reaction mechanisms and implications for phosphorus reclamation and recycling. Submitted.

Conference Presentations

- Rixiang Huang, Yuanzhi Tang. Transformation of nitrogen and phosphorus during (hydro)thermal treatments of biosolids. American Chemical Society (ACS) Conference. Philadelphia, PA (2016/08)
- Rixiang Huang, Yuanzhi Tang. Speciation dynamics of metals and phosphorus during (hydro)thermal treatments of sewage sludge. American Chemical Society (ACS) Conference. San Diego, CA (2016/03).

References

1. Hedley, M.J., J. Stewart, and B. Chauhan, *Changes in inorganic and organic soil phosphorus fractions induced by cultivation practices and by laboratory incubations*. Soil Science Society of America Journal, 1982. 46(5): p. 970-976.
2. Mossop, K.F. and C.M. Davidson, *Comparison of original and modified BCR sequential extraction procedures for the fractionation of copper, iron, lead, manganese and zinc in soils and sediments*. Analytica Chimica Acta, 2003. 478(1): p. 111-118.
3. Huang, R. and Y. Tang, *Speciation Dynamics of Phosphorus during (Hydro)Thermal Treatments of Sewage Sludge*. Environmental Science & Technology, 2015. 49(24): p. 14466-14474.
4. Kar, G., L.S. Hundal, J.J. Schoenau, and D. Peak, *Direct Chemical Speciation of P in Sequential Chemical Extraction Residues Using P K-Edge X-Ray Absorption Near-Edge Structure Spectroscopy*. Soil Science, 2011. 176(11): p. 589-595.
5. Oxmann, J.F., *Technical Note: An X-ray absorption method for the identification of calcium phosphate species using peak-height ratios*. Biogeosciences, 2014. 11(8): p. 2169-2183.

Geostatistical Models for Optimizing Groundwater Monitoring Network in the Lower Apalachicola-Chattahoochee-Flint (ACF) River basin

Basic Information

Title:	Geostatistical Models for Optimizing Groundwater Monitoring Network in the Lower Apalachicola-Chattahoochee-Flint (ACF) River basin
Project Number:	2016GA365B
Start Date:	3/1/2016
End Date:	1/31/2017
Funding Source:	104B
Congressional District:	5
Research Category:	Ground-water Flow and Transport
Focus Category:	Groundwater, Management and Planning, Models
Descriptors:	None
Principal Investigators:	Jian Luo

Publications

There are no publications.

FINAL REPORT

Geostatistical Models for Optimizing
Groundwater Monitoring Network in the
Lower Apalachicola-Chattahoochee-Flint
(ACF) River Basin

Jian Luo

**School of Civil and Environmental Engineering
Georgia Institute of Technology**

Contents

Abstract:	2
1. Introduction:	3
2. Scope and Objectives:	6
3. Experiment under consideration:	6
4. Need for separating the field:	8
5. Random fields and variogram behavior.....	10
5.1 Variogram shifting when the points from different fields are added	11
5.2 Range of variogram deviation	13
6. Least Variogram Deviation Algorithm.....	18
7. Initial clusters	21
8. Summary and Conclusion.....	23
9. Future work.....	24
Acknowledgement	25
References.....	25

Abstract:

Groundwater is the vital water source in the lower Apalachicola-Chattahoochee-Flint (ACF) River basin in southwestern Georgia. The main objective of this study is to enhance the accuracy of the kriging estimates by separating random fields and performing kriging using multiple correlation structures that are prevail in the measurements of groundwater usage and levels in the ACF River Basin. It was found that the estimates using constituent random fields gives much more accurate kriging predictions compared to using single mixed random field. The novel cutting edge technique based on the variogram deviation was developed to identify and separate the different correlation structures in a potential mixture of fields. The two stage technique involves obtaining the initial cluster from random sampling followed by *least variogram deviation* algorithm for the assignment of the remaining points. Given the initial pure cluster, the second stage of the method performed excellently with highly accuracy of classification. However, the first stage of getting the initial clusters through random sampling is not very reliable and need further improvement. The proposed clustering technique with further improvement can lead to a significant improvement in the studies of optimizing the pumping well monitoring network and estimating the groundwater withdrawals for irrigation in the ACF River Basin.

1. Introduction:

Groundwater is the major source of water in the lower Apalachicola-Chattahoochee-Flint (ACF) River basin in south-western part of Georgia [Albertson and Torak, 2002; Leeth et al., 2005; Fanning, 1997, 2003; Mosner, 2004; Warner and Stephen, 2005]. With the large scale withdrawals of groundwater for the irrigation in the region, it becomes very important to continuously monitor the pumping from the wells to get the clear and accurate estimate of amount and pattern of water extracted. These estimates lead to the evaluations of hydrologic aquifer stress, which is crucial factor to consider in long term sustainable water resource management plans. Following a State Legislature in June 2003, Georgia Soil and Water Conservation Commission (GSWCC) installed more than 10,000 annually read water meters and around 200 daily reporting telemetry sites on irrigation systems primarily in southern Georgia (2004 to 2010) in order in monitor agricultural withdrawals [Torak and Painter, 2011]. However due to budget constraints and large number of pumping wells in the study area, it is not possible to install meter at every well. Further due to budget cuts, it is getting difficult to operate and maintain even the existing monitoring network. Thus, there is a pressing need for optimizing the existing monitoring network to maximize the useful information with minimum monitoring efforts. In addition to monitoring the extraction at selected wells, there is a need for the comprehensive and robust procedure to estimate the groundwater usage over the whole study region, necessitating the efforts to develop indirect method for irrigation withdrawal estimate using the data from the metered sites. With the objective of providing water resource managers and policy makers a comprehensive information about water consumptions, losses and transfers, U.S. Geological Survey (USGS) established the National Water Census authorized by section 9508 of the secure water action of 2009 [Painter et al., 2015].

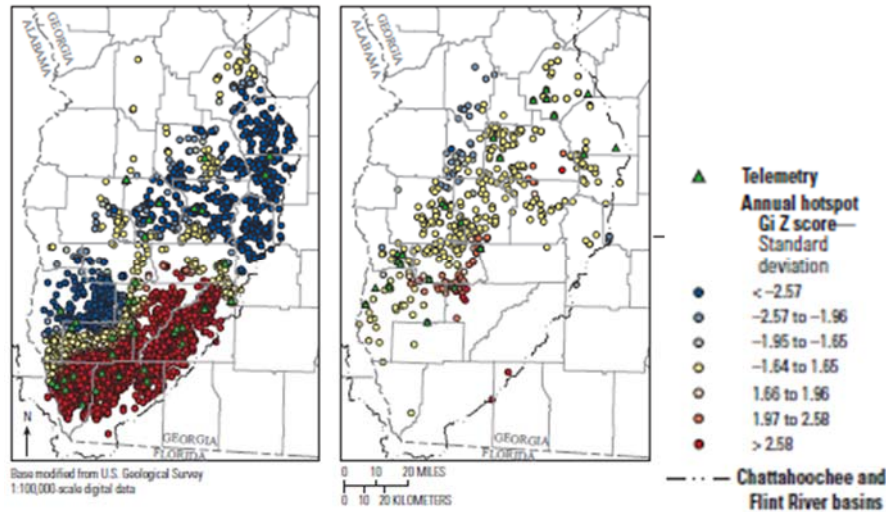


Figure 1: Standard deviation distribution of Getis Ord Gi statistic resulting from hot-spot analysis of annually reported irrigation water-meter data for (A) groundwater and (B) surface water, and corresponding telemetry networks for the middle and lower Chattahoochee and Flint River basins, 2007 [Torak and Painter, 2011]

Painter *et al.* (2015) evaluated the estimation techniques using nationally available data-sets, described herein – the crop-demand method, geostatistical technique, and image analysis, for the estimate of total irrigation withdrawal in ACF river basin focus area. They found that none of these techniques prove to be a turnkey method to estimate irrigation withdrawals. The crop-demand method requires data parameterization of soil, crop and meteorological data which undermines the site-specific conditions and affect the estimations. Painter *et al.* (2015) suggested that geostatistical technique can potentially produce most dependable and consistent estimates requiring minimal parameterization. However, accuracy of geostatistical estimates is largely dependent on accurate meter reading of irrigated volumes and associated irrigated acres. Crop-demand model and geostatistical technique, both suffer from the inconsistencies and inaccuracies in the estimation of the irrigated acres, which turns out to be the most critical parameter for the accurate estimate of the irrigation withdrawals. Image analysis, which is primarily aimed at getting monthly estimates of the irrigated areas prove to be inadequate due to inconsistent satellite imagery caused by atmospheric interferences [Painter *et al.*, 2015].

Geostatistical technique turns out to be a very attractive and viable method as it requires minimal parameters (data driven) and it has higher considerations for the site specific conditions

compared to other techniques evaluated by *Painter et al.* (2015). Favoring it further, a huge amount of resources is being invested in the metering program which provides necessary data set for geostatistical analysis. *Torak and Painter* (2011) used geostatistical techniques which include variogram analysis, kriging and cross-validation, of the annually reported meter data. The objective was to evaluate the spatial correlation structure and employing it to revise the telemetry meter distribution, thus reducing the estimation errors associated with using telemetry network to represent the annually reported meter data. They suggested that careful selection of the distance class to obtain experimental variogram yielded strong spatial correlation of the water meter data with distance. The exponential variogram model fitted by them to the experimental variogram showed a very good fit with the R-squared value equal to 0.998. However, it is important to note that fitting a variogram model to the experimental variogram is not same as fitting the estimation model to the originally known data. A parameters yielded from a good agreement between the model to the experimental variogram does not imply good estimations of data points. It is the residuals of the estimation that are important to evaluate the adequacy and accuracy of the model, making it imperative to use residual statistics as a criterion to select or reject the variogram model. Moreover, it is important to recognize the non-homogeneity of the data, since data has a clear trend from north-west to south-east in the region of interest as seen in Fig 1. This trend was not considered in the analysis. Also there is a possibility that data points from all the meter locations in the study region may not represent a single correlation structure but rather can be explained better by using multiple correlation structures, which may be existing due to different aquifer layers in which the wells are screened, the crop type and other regional factors. In such cases, using the whole dataset to obtain single variogram model, which when used for kriging estimates, can lead to significantly high errors compared to deploying multiple correlation structures for kriging. Therefore, there is a need for the technique to identify and separate the random fields from the mixed field. The random fields with significantly different constant means or fields which are spatially isolated can be separated using K-means clustering. However, we do not have this prior information and also when the means of the random fields are not much different and there is an overlap in the range of data values, the fields become indistinguishable for the conventional techniques, suggesting a need for a more robust technique that can separate field for a variety of differences in the correlation structures.

In this study we attempt to develop a novel technique to identify and separate potential multiple correlation structures in the dataset. The developed technique will be tested over a wide range of scenarios using the synthetically developed mixed random fields. The effectiveness of the technique is evaluated using the purity of the clustered fields with respect to the original fields.

2. Scope and Objectives:

Scope of this study is limited to the mixture of two fields with equal contribution from both the fields. However, it will be extended to more than two fields and other complexities in the future. The main objective of this research is to develop the tools to enhance the kriging estimates by separating the potentially mixed field. The main steps involved in the study are:

- 1) Perform numerical experiments to study the effect of mixing fields on variograms and kriging residuals
- 2) Propose new approaches to separate the mixed fields
- 3) Test and compare the proposed approaches

3. Experiment under consideration:

A rectangular study area is considered with the dimensions 100 units by 50 units. 3000 random locations were selected for data points, 1500 for each of two random fields. The data locations are populated with data values using unconditional simulations governed by two different variogram models. An example of the same is presented in Figure 2 showing pixelated data field, Figure 3 showing the experimental variograms of the original fields and the mixed field and Figure 4 showing the histogram of the data. Our aim is to obtain the original fields with good accuracy to enhance the kriging estimates over using the whole mixed field.

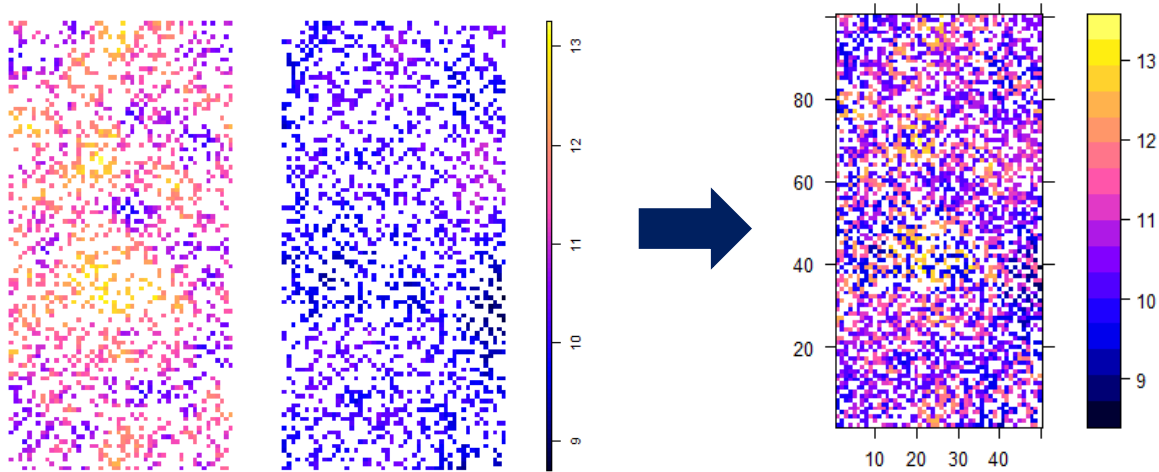


Figure 2: Pixelated data values of original fields and the mixed field. Field 1: Exponential variogram with mean 11, sill 0.50 and range 10. Field 2: Exponential variogram with mean 10.5, sill 20 and range 10.

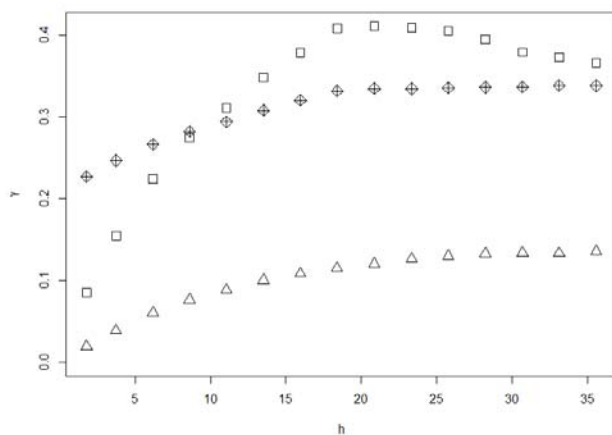


Figure 3: Experiment variogram of the original constituent fields and mixed field

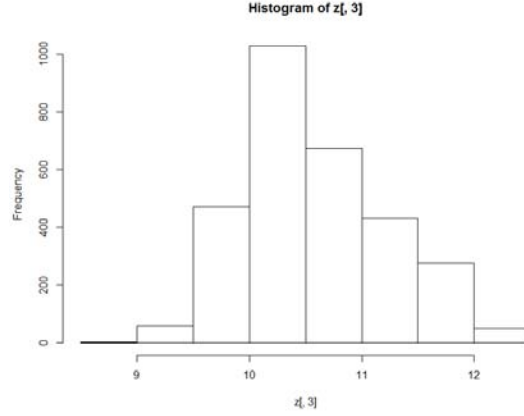


Figure 4: Histogram of the mixed field

4. Need for separating the field:

Since, our final objective is to get kriging estimates with good accuracy using the spatial correlation structure of the given dataset, it is important to justify the efforts we put in to identify and separate the correlation structures. We consider the case described in Sec. 3. We first consider the whole field, plot a single experimental variogram, fit variogram model and then perform 100-fold cross-validation (CV) to get kriging residual errors. We then repeat the mentioned steps using the original two fields and obtain the kriging residual errors. The fitted model parameters are presented in Table 1, and experimental and fitted variograms are shown in Figure 5 and Figure 6. The CV errors are presented in the form of Mean Absolute Error (MAE) and Root Mean Square Error (RMSE) in Table 2.

Table 1: The variogram model parameters of mixed and individual fields

	Nugget	Type	Sill	Range
Mixed field	0.21	Exponential	0.36	11.15
Original field 1	-	Exponential	0.42	7.90
Original field 2	-	Exponential	0.15	11.59

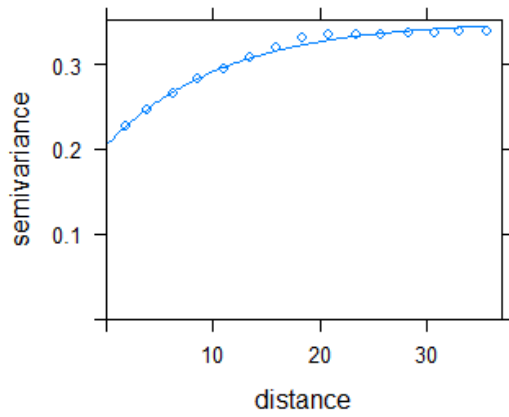


Figure 5: Experimental variogram and fitted variogram model taking all the data points together as single mixed field.

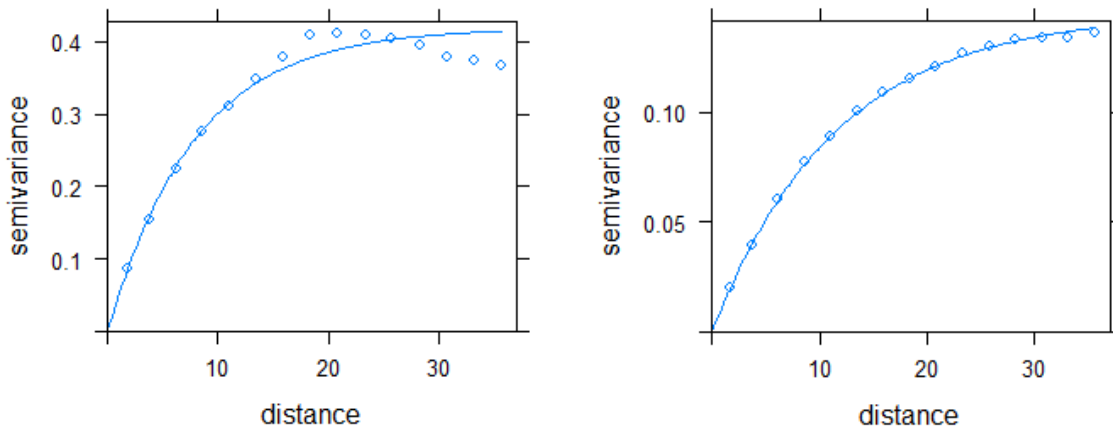


Figure 6: Experimental variogram and fitted variogram model by considering the constituent fields separately

Table 2: The residual error after 100-fold Cross Validation

	MAE	% MAE	RMSE	% RMSE
Original 2 Fields	0.1384	-	0.1834	-
Mixed Single Field	0.4473	223%	0.5407	194%

As we can see from the CV results, using the whole field to perform variogram analysis and kriging leads to significant loss in the accuracy of kriging estimates compared to using the original fields. Therefore, there is a strong incentive in separating the constituent random fields from the mixed field to get accurate kriging predictions. However, given the information we would have is only the mixed field dataset, the task of separating the constituent fields is really challenging. We have got some good leads in our efforts in this direction, which are discussed in the following sections.

5. Random fields and variogram behavior

Field which are spatially isolated or having no overlap in the range of their values can be separated using the conventional techniques like K-means. However, fields with the overlapping areal domain and range of values pose a great challenge for the identification and separation of constituent fields. Difference in such fields can be different correlation length (range) or sill (variance). Therefore, variogram based classification/clustering approach is needed for such cases.

The central idea behind our approach is the different deviations occur in variograms when points from different fields are added. In this section, we analyze the behavior of variograms under different scenarios of field mixing which can be used as clues about field, the added point might be belonging.

5.1 Variogram shifting when the points from different fields are added

The considered random fields and their experimental variograms are presented in Figure 7 and 8.

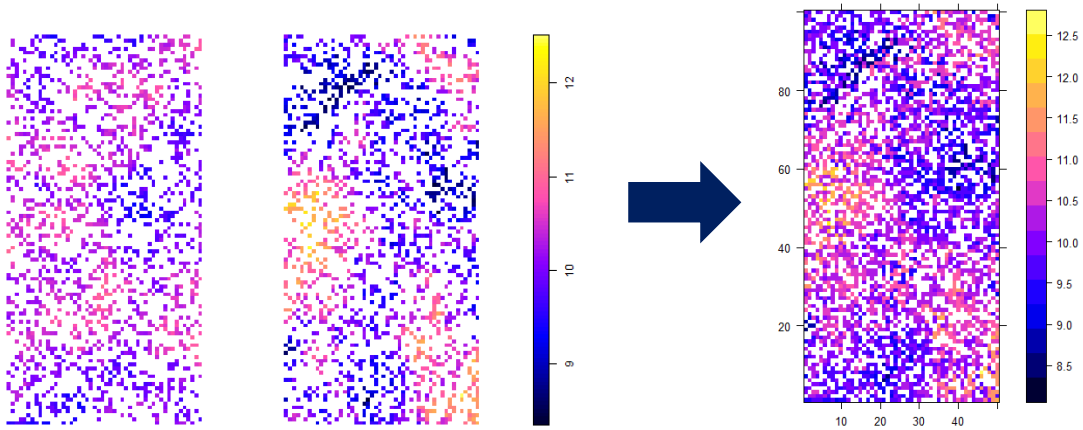


Figure 7: Two fields are merged to form the mixed field. Field 1: Exponential variogram with mean 10, sill 0.50 and range 10. Field 2: Exponential variogram with mean 10, sill 0.25 and range 20.

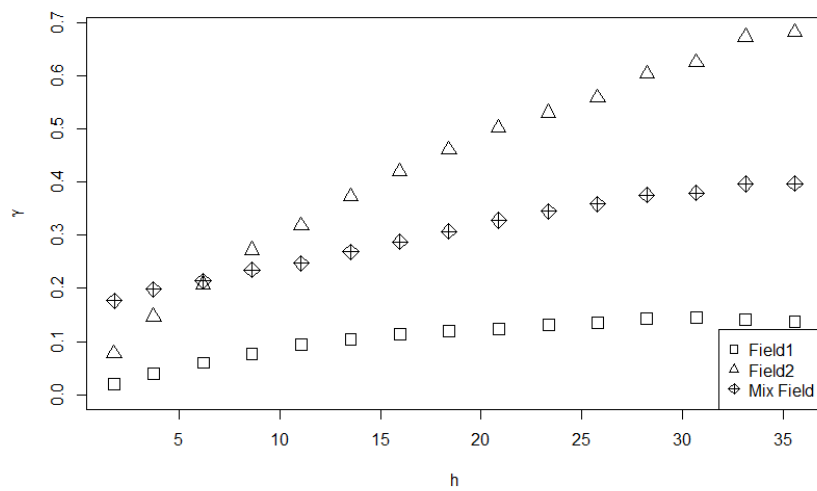


Figure 8: Experimental variograms of the original fields and mixed fields

We started with the sample of 500 randomly selected points from each fields which we would call as pure initial clusters. We made these clusters increasingly impure by adding one point at time from other field, and we observed the movement of the variograms with the increasing impurity. We compared this with the case where we continuously added points to these pure initial clusters from the field they belong. As we can see in Figure 9 and 10, variograms after 50th, 250th, 400th and 500th point is added to the initial cluster, the variogram moves closer to each other as points from the other field are added. Eventually when both the clusters have equal number of points from both the fields (50% purity), the variograms tend to be identical. Therefore, it would not be wrong to say, more distant the variograms are, more pure they are.

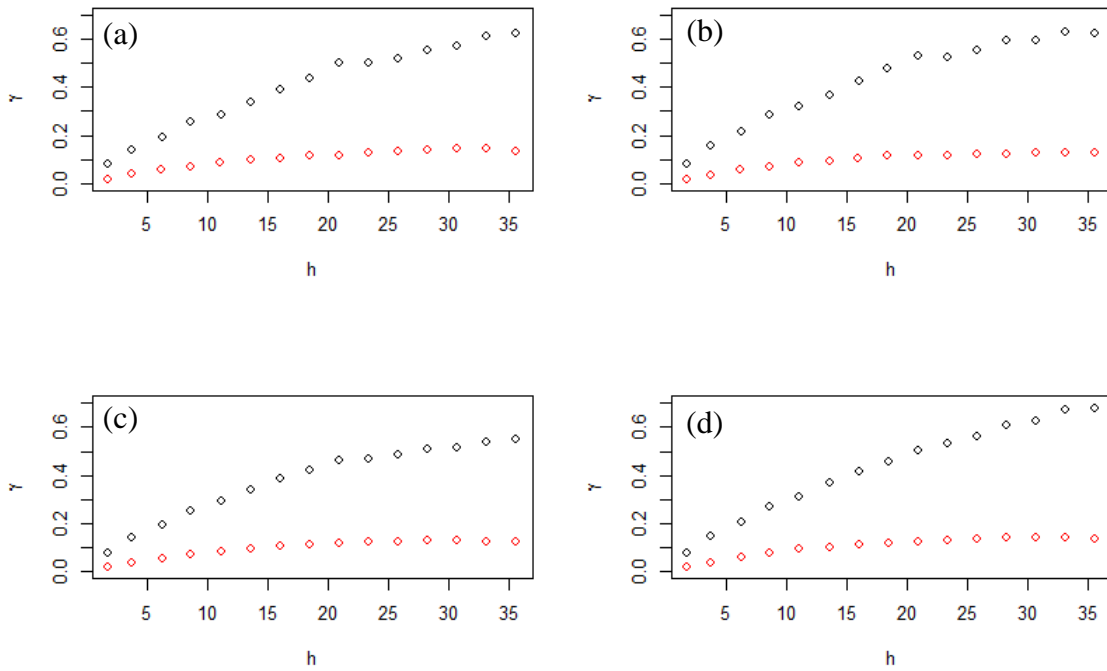


Figure 9: Variograms after 50th (a), 250th (b), 400th (c) and 500th (d) point from the same field are added to the initial pure clusters, maintaining the purity equal to 100%

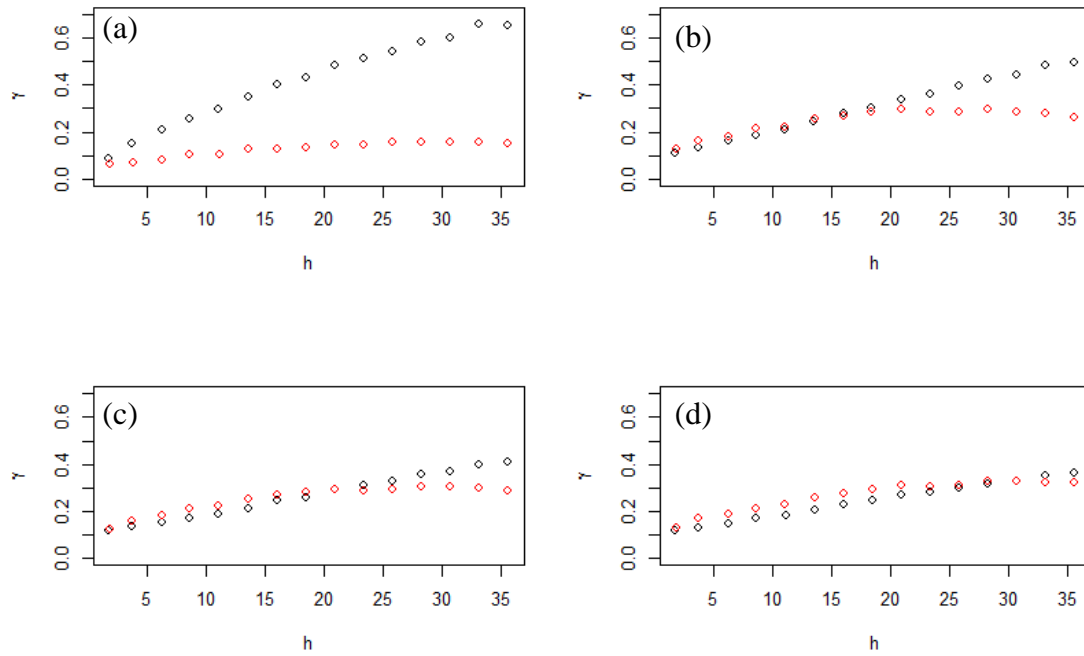


Figure 10: Variograms after 50th (a), 250th (b), 400th (c) and 500th (d) point from the other field are added to the initial pure clusters, continuously decreasing the purity from 100% to 50%

5.2 Range of variogram deviation

As we saw in the previous section, the deviations in the variograms are different on adding points from different field. It is expected that if the added point is from the same field, the variogram will tend remain unchanged, and if the added point is from the different field, there would be a significant deviation in the variogram. Therefore, to get the range of these deviations we try to obtain the band of variograms deviation by adding with replacement, points from the same field and other field to the initial pure clusters. We consider two cases, one with different sills and another with different ranges, keeping means same in both the cases.

Case 1: Different sill

The two fields with different sills i.e. 0.15 and 0.50, while keeping mean as 10 and range as 10 for both the fields are considered. Figure 11 (a) shows their pixelated values Figure 11 (b) their experimental variograms. We begin with we take pure samples of 400 points from each field.

Variograms corresponding to these initial pure clusters are shown in Figure 12. We added one randomly selected point from field 1 to both the clusters to obtain updated variograms. We repeated this 100 times, with every time removing the previously added point before adding the new point, to get a band of variograms. We got similar band of variograms by adding points from field two.

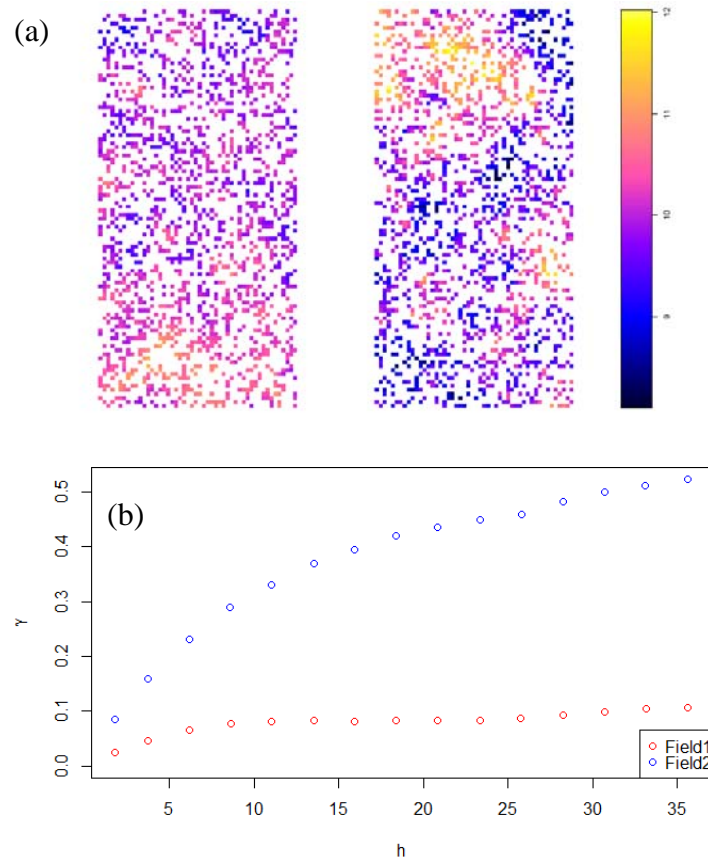


Figure 11: Random fields with different sill but same mean and range (a) pixelated z values in space; (b) experimental variograms of the field

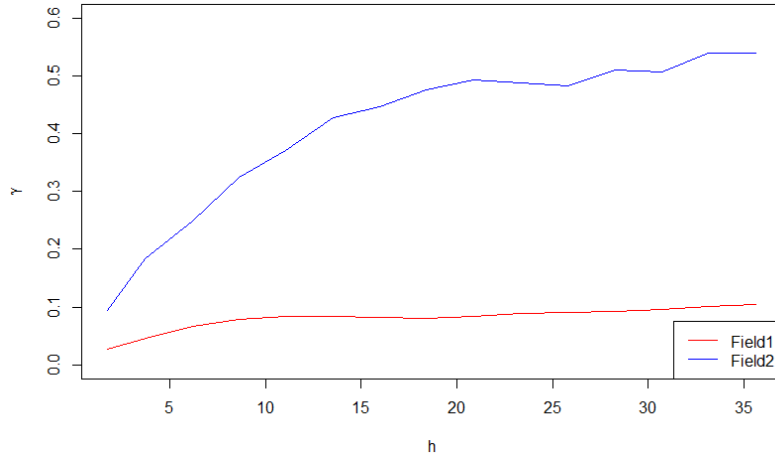


Figure 12: Variograms of initial pure clusters with 400 points each

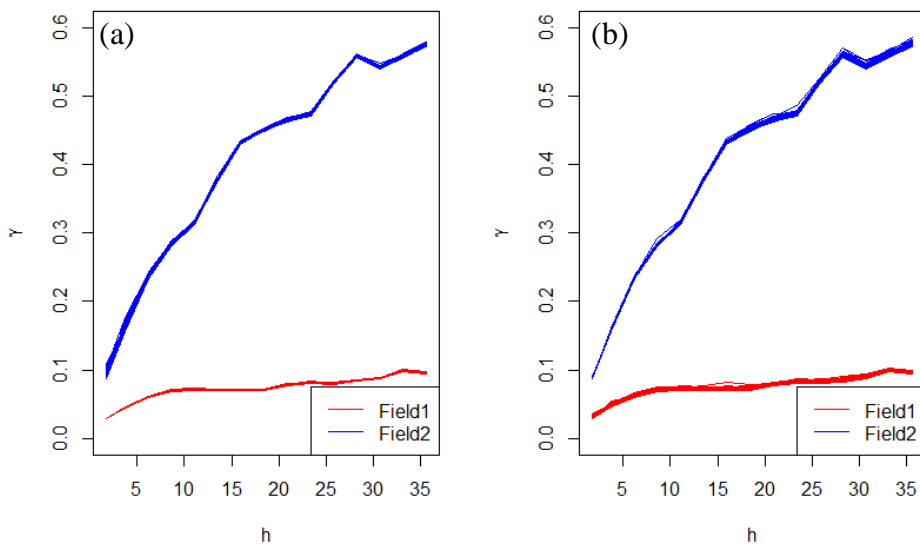


Figure 13: Band of variogram deviations when points from: (a) Field 1 were added; (b) Field 2 were added

Case 2: Different Range

The two fields with different ranges as i.e. 5 and 25, while keeping mean as 10 and psill as 0.25 for both the fields are considered. Figure 14 (a) shows their pixelated values Figure 14 (b) their experimental variograms.

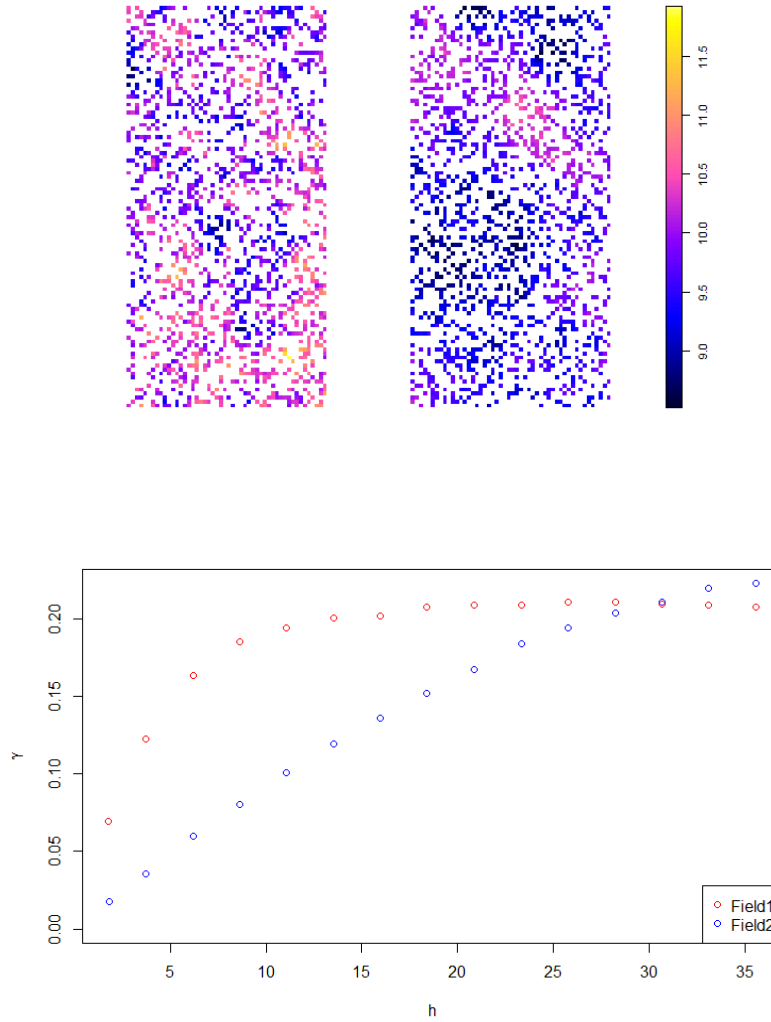


Figure 14: Random fields with different range but same mean and range (a) pixelated z values in space; (b) experimental variograms of the field

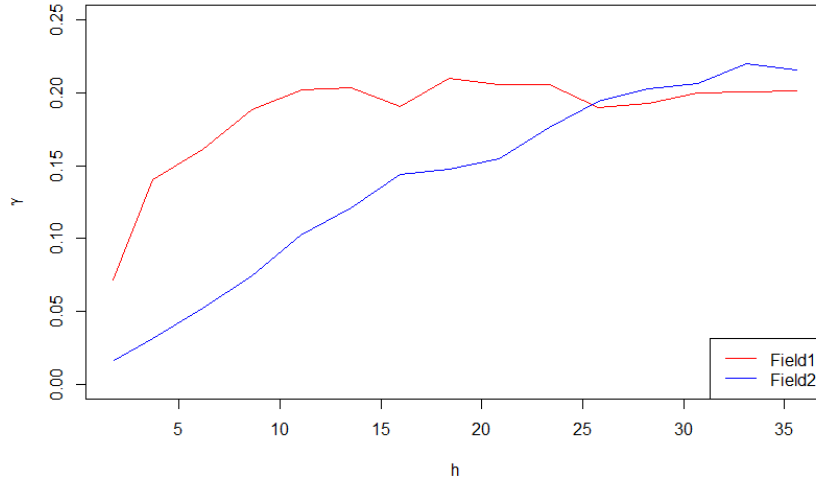


Figure 15: Variograms of initial pure clusters with 400 points each

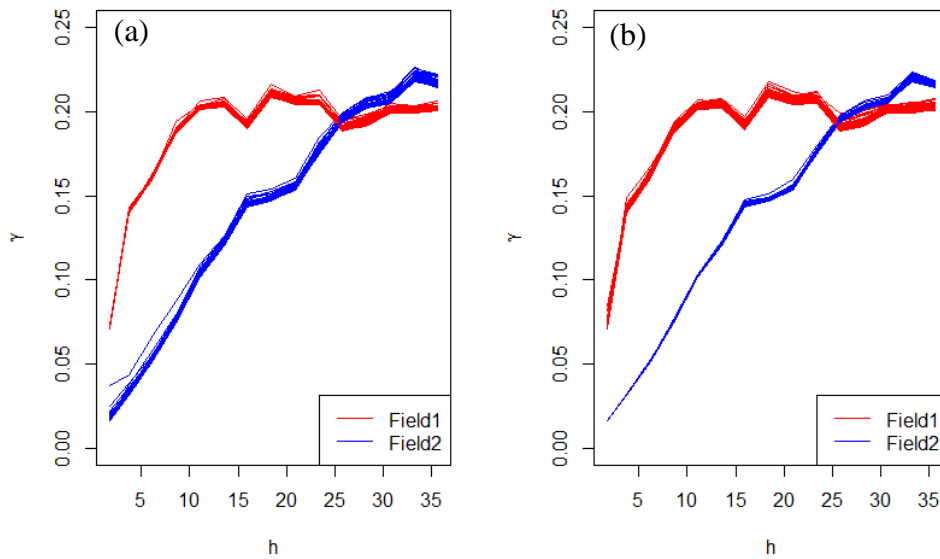


Figure 16: Band of variogram deviations when points from: (a) Field 1 were added; (b) Field 2 were added

As we can see in Figure 13 and 16, the band of variogram deviation is thicker if the added points come from the different correlation structure compared to if the added points belong to the same correlation structure. This property can play a crucial role in clustering of the data points based on variogram. Based on this we developed a novel technique, least variogram deviation

algorithm, to assign the points to the cluster representing the correlation structure they come from. However, this algorithm works with the condition that we have initial cluster with good purity to start assigning the remaining points. However, getting these initial clusters in dealt separately in Sec 7. In the next section, we present the results and sensitivities of the least variogram deviation algorithm.

6. Least Variogram Deviation Algorithm

To evaluate the performance of the developed least variogram deviation algorithm with the given initial pure clusters, we consider the mixture of the following fields: **Field 1**: “Exponential”; Mean= 10; Sill=0.25; Range= 20; **Field 2**: “Exponential”; Mean= 10; Sill=0.50; Range= 10. We have 3000 data point in total, 1500 from each field (Section 5.1).

To apply least variogram deviation algorithm, we consider 600 points from both the field as perfect initial clusters (100% percent). After assigning the remaining 1800 points to clusters using the proposed variogram based clustering algorithm, the purity of the final clusters excluding the initial pure clusters was found to be 80%. Figure 17 shows the excellent match between the spatial correlation structures represented by the clustered fields and original constituent fields of the dataset.

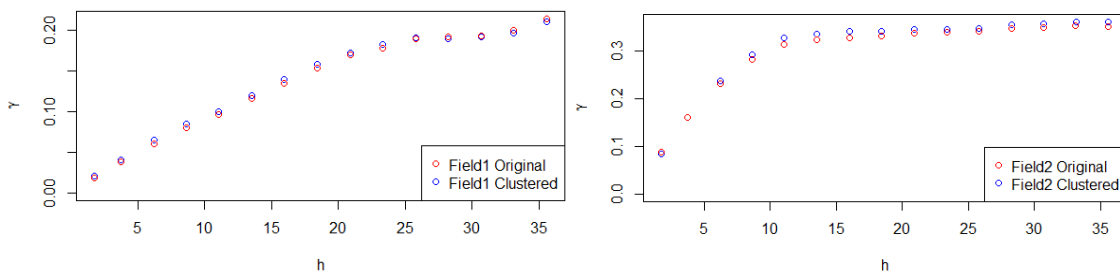


Figure 17: Comparison of experimental variograms of final clusters and original fields; 600 points in initial clusters

However, it is crucial to remember that we used pure initial cluster as seed to the algorithm. Therefore it is important to assess the sensitivity of the effectiveness of the algorithm to the size of the initial cluster. Table 3 presents the purity of the final clusters (excluding the initial pure

clusters) for different sizes of the initial clusters. To put in perspective, if we have initial clusters of size 100 points each, the remaining 2800 points can be assigned to the clustered with the accuracy of 72%. It is also important to note that, as we decrease the size of the initial clusters from 600 to 100 with decrements of 100 points, the first significant drop in the final cluster purity was observed at 300 size i.e., size equal to the 10% of the total dataset size. Figure 18 shows the comparison of variograms of final clusters (72% purity) obtained using least variogram deviation technique with 100 points each in initial clusters. Figure 18 compares the experimental variograms of the final clusters.

Table 3: Sensitivity of the least variogram deviation algorithm results to the initial cluster size.

Initial Cluster Size	Final Clusters Purity
(600,600)	80%
(500,500)	79%
(400,400)	80%
(300,300)	76%
(200,200)	74%
(100,100)	72%

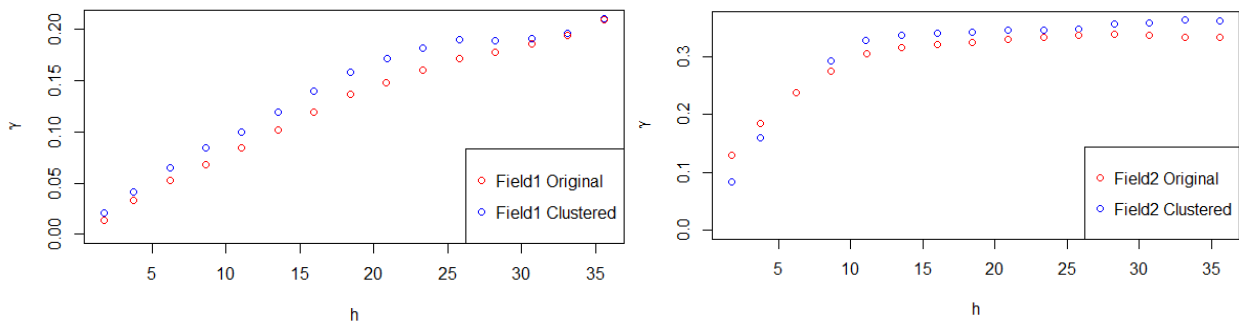


Figure 18: Comparison of experimental variograms of final clusters and original fields; 100 points in initial clusters

We also assessed the sensitivity of the algorithm to the difference in variogram model parameters of original constituent fields. Taking 400 points in each initial pure cluster, we assigned the

remaining 2200 points using least variogram deviation algorithm. Because of the stochastic nature of the experiments, we repeated each experiment 4 time. Table 4 and Table 5 presents the final cluster purities for different sill differences and range differences, respectively.

Table 4: Sensitivity of algorithm performance to sill difference of original constituent fields with range as 10 and mean as 10 for both fields

Sills	Final Clusters Purity			
(0.40, 0.50)	69%	80%	71%	73%
(0.25, 0.50)	79%	77%	72%	78%
(0.10, 0.50)	72%	74%	75%	72%

Table 5: Sensitivity of algorithm performance to range difference of original constituent fields with sill as 0.5 and mean as 10 for both fields

Ranges	Final Clusters Purity			
(5, 10)	71%	65%	72%	72%
(5, 20)	72%	75%	75%	77%
(5, 30)	76%	72%	74%	71%

As we can see from the Table 4 and 5, as far as the variograms are significantly different, there is no significant improvement in the performance with increasing difference in the variogram model parameters. In the next section, we attempt to get initial clusters.

We analyzed the misclassified points and found that these points are statistically same for spatial correlation structures represented by both clusters and hence they effect both the variograms similarly. We performed numerical experiments similar to Sec. 5.2. Since, we know the original fields of the misclassified points, we add these points to the pure variogram of original fields and assess the difference it makes. As we can see in Figure 19, these points satisfy both correlation

structures equally well. Since, these points do not distort the correlation structure of original fields, their misclassification is not expected to affect the kriging results.

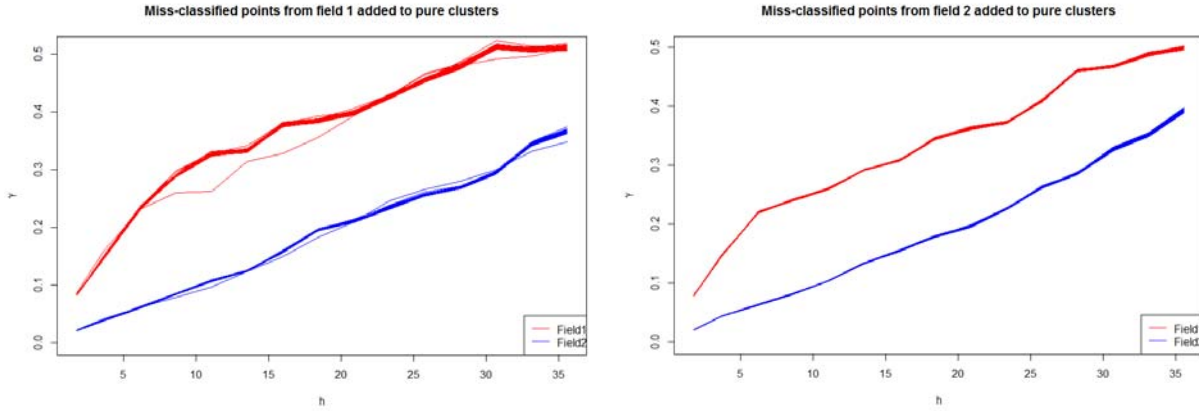


Figure 19: Variogram deviation band obtained by adding miss-classified points to the pure variograms

7. Initial clusters

The least variogram deviation algorithm requires initial clusters to assign the remaining points. However, our analysis in the previous section is based on using pure initial clusters from the known original fields. In this section, we suggest a way to get the initial clusters from the dataset representing the mixed field.

As discussed in Sec. 5.1, with the increasing impurity of the two clusters, the variograms move closer and become less and less different. Based on this idea, we randomly pick 5 to 10 mutually exclusive samples from the dataset and plot their experimental variograms. We retain the most apart variograms. We pick new samples and retain the most apart variograms. The distance between variogram pair of this sample is compared with previously retained pair and, the variogram pair with higher distance is retained. This process is repeated for 1000 times and finally we get initial clusters.

We again consider the case of same mean but different variogram model parameters, as considered in Sec. 5.1 and presented in Figure 7 and 8. Figure 20 presents a quick look at the

variograms of picked 5 random samples. As expected, the variograms of samples look very similar to the variogram of the mixed field (Figure 21), as the random sample tend to have equal proportion from both the constituent fields. This method relies on the fact that, when the sampling is repeated 1000 times, there is a chance that biased sample will be picked having significantly higher proportion of points from one field than other which will be retained by our set criteria based on variogram distance. The purity of initial clusters for different sample sizes and number of samples are presented in Table 6. The smaller sample size results in better initial clusters as there is higher chances of getting a biased sample for small size of sample. Sample size of 50 resulted in 71% purity of the initial clusters obtained. However, as we already seen in Table 3, smaller initial clusters results in lesser purity of final cluster obtained using least variogram deviation algorithm. Largest sample size, 300, yielded lowest initial cluster purity which also hampers the results of least variogram deviation technique.

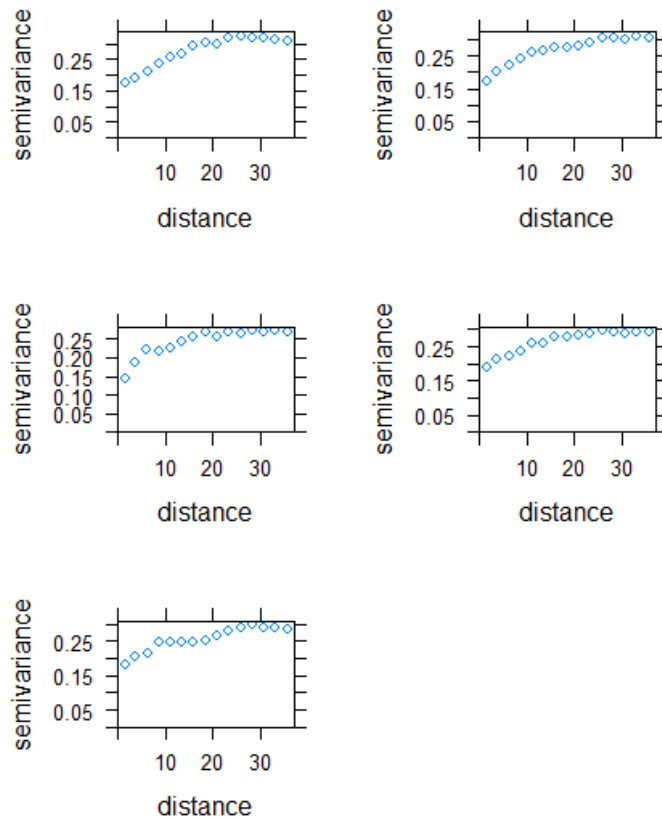


Figure 20: Variograms of random samples from the dataset

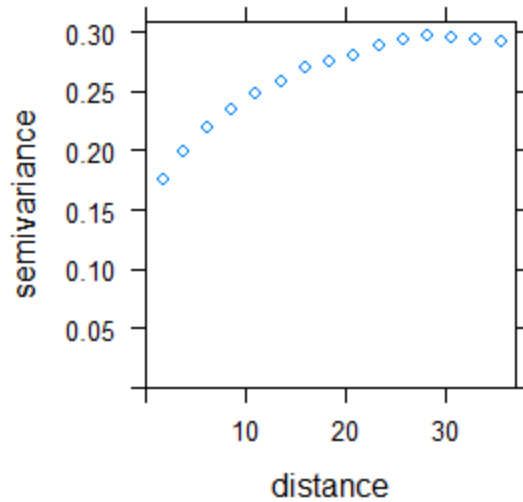


Figure 21: Variograms of the mixed field

Table 6: Initial cluster purities for different sample size and number of samples

(Sample Size, No. of samples)	No. of iterations	Purity of Initial cluster
(100,5)	1000	66%
(300,10)	1000	59%,
(200,10)	1000	60%
(100,10)	1000	65%

8. Summary and Conclusion

It is very common in geohydrology of to perform variogram analysis considering single random field for the whole dataset. In the previous studies performed for optimizing the groundwater pumping monitoring network and estimation of groundwater withdrawals for the irrigation in the Apalachicola-Chattahoochee-Flint River Basin, single variogram model was used to represent the correlation structure of the whole dataset. However, there is no clear evidence provided regarding why using the single correlation structure is a suitable for such studies. On the other

hand, the quite apparent trend in the data, existence of three different aquifer layers and other heterogeneities strongly incentivize the need to examine the existence of multiple correlation structures governing the pumping values in the dataset. In this study also, we showed using synthetic data that in the case of existence of multiple fields, the variogram analysis and kriging assuming single field can lead to higher prediction errors. In this study we proposed novel variogram based techniques to identify different correlation structures and clusters the data points according to them.

Fields which are spatially distinct or which have no overlap in the range of data values can be separated using K-means clustering. However, challenging cases are where the random fields have overlapping spatial domain and also have same means or significant overlap in the ranges of data values. Separating such fields requires spatial correlation based technique. In this study we proposed a two-step method of getting initial clusters followed by least variogram deviation algorithm to assign the remaining points. Obtaining initial clusters through random sampling is based on the chance of getting a biased sample and can work for small size of sample only (~ 100 to 200 points). However, stochastic nature of this technique makes it unreliable and there is a need for more theory based robust technique to get initial clusters. The second stage clustering which assigns the remaining points performed well and clustering the unassigned points with the accuracy of 80% with the pure initial clusters. The misclassified points were found to be statistically similar and would have similar effects on variogram when added to either of the field. Hence, their misclassification would not any significant negative effect on the kriging estimates.

9. Future work

This study exposed the huge potential of clustering based kriging and also revealed that even the overlapping random fields with same mean can be separated by using suitable variogram based clustering technique. The major immediate advancement planned for this study includes:

- 1) More robust technique to obtain initial clusters;
- 2) Addressing the case of different proportion of data points from the constituent random fields;
- 3) Applying the proposed technique to groundwater head or pumping datasets in the ACF River Basin;

- 4) Addressing the possibility of separating the mixed field constituted by more than two random fields.

Acknowledgment

The authors thank to the support from Georgia Water Resources Institute and the Director Dr. Georgakakos. Their help and guidance facilitates the completion of the study. Saubhagya Singh Rathore, a graduate student supported by the funds, conducted most of the research.

References

- Albertson, P.N., and L.J. Torak, Simulated effects of ground-water pumpage on stream-aquifer flow in the vicinity of federally protected species of freshwater mussels in the lower Apalachicola-Chattahoochee-Flint River basin (subarea 4), southeastern Alabama, northwestern Florida, and southwestern Georgia, U.S. Geological Survey Scientific Investigations Report 02-4016.
- Fanning, J.L., Water use in Georgia by county for 1995: Georgia Geologic Survey Information Circular 101, 1997.
- Fanning, J.L., Water use in Georgia by county for 2000 and water-use trends for 1980 – 2000: Georgia Geologic Survey Information Circular 106, 2003.
- Leeth, D.C., J.S. Clarke, C.J. Wipperfurth, and S.D. Craig, Ground-Water Conditions and Studies in Georgia, 2002– 03, Scientific Investigations Report 2005-5065, 2005.
- Mosner, M.S. Stream-aquifer relations and the potentiometric surface of the upper Floridan aquifer in the lower Apalachicola-Chattahoochee-Flint River basin in parts of Georgia, Florida, and Alabama, 1999-2000, U.S. Geological Survey Investigations Report 02-4244.
- Painter, J. A., Torak, L. J., & Jones, J. W. (2015). Evaluation and comparison of methods to estimate irrigation withdrawal for the National Water Census Focus Area Study of the Apalachicola-Chattahoochee-Flint River Basin in southwestern Georgia (No. 2015-5118). US Geological Survey.

Torak, L. J., & Painter, J. A. (2011). Summary of the Georgia Agricultural Water Conservation and Metering Program and evaluation of methods used to collect and analyze irrigation data in the middle and lower Chattahoochee and Flint River basins, 2004-2010. U. S. Geological Survey.

Warner, D., and J. Stephen. Lawrence Ground-Water Flow and Water Quality in the Upper Floridan Aquifer, Southwestern Albany Area, Georgia, 1998–2001 U.S. Geological Survey Scientific Investigations Report 2005-5047, 2005.

Fecal bacteria source tracking, nutrient analysis, and modeling of an urban TMDL watershed

Basic Information

Title:	Fecal bacteria source tracking, nutrient analysis, and modeling of an urban TMDL watershed
Project Number:	2016GA366B
Start Date:	4/1/2016
End Date:	7/31/2017
Funding Source:	104B
Congressional District:	GA-10
Research Category:	Water Quality
Focus Category:	Non Point Pollution, Surface Water, Models
Descriptors:	None
Principal Investigators:	David Radcliffe, Mussie Ykeallo Habteselassie

Publications

There are no publications.

Fecal bacteria source tracking, nutrient analysis, and modeling of an urban TMDL watershed;
Radcliffe, D. and Habteselassie, M.; University of Georgia.

The Georgia Water Resources Institute asked for and received permission to extend the deadline of this research project into FY2016 to allow the PIs to make field measurements that could not have been completed by the original project deadline. The final project report will be included in the FY2017 Annual Report.

Comparison of Oconee and Ocmulgee river basins for sustainable ecosystem and economic development of Middle Georgia

Basic Information

Title:	Comparison of Oconee and Ocmulgee river basins for sustainable ecosystem and economic development of Middle Georgia
Project Number:	2016GA367B
Start Date:	3/1/2016
End Date:	2/28/2017
Funding Source:	104B
Congressional District:	10th
Research Category:	Climate and Hydrologic Processes
Focus Category:	Hydrology, Models, Management and Planning
Descriptors:	None
Principal Investigators:	Ernest W Tollner, Todd Rasmussen, Abhyuday Mandal

Publications

There are no publications.

Comparison of the Middle Oconee and the Middle Ocmulgee rivers for sustainable ecosystem and economic development of Middle Georgia

Natalia V. Bhattacharjee (née Shim)¹, Ernest W. Tollner¹, Abhyuday Mandal² and Todd C. Rasmussen³

¹College of Engineering, University of Georgia; ²Department of Statistics, University of Georgia ³Warnell School of Forestry and Natural Resources, University of Georgia

Motivation

With increasing population in Middle Georgia, water demand and wastewater generation are dramatically increasing. This requires refining water management strategies to meet future demands and support economic development of the region. The Oconee River and Ocmulgee River are adjacent basins and major tributaries that join to form the Altamaha River. River flow in these rivers is affected by Wallace Dam and Lloyd Shoals Dam that are located near Oconee Lake and Jackson Lake, respectively. Our study examines the ecological effects of alternative water management practices in both the Oconee and Ocmulgee river basins. These rivers harbor high aquatic biodiversity, and protecting these species is of high priority for the region. Thus, we simulate alternative environmental flow regimes and examine trade-offs in water management between ecological impacts and economic development. Our analysis of how reservoir operation can influence local hydrology and fish habitat can provide information for sustainable ecosystems and economic development along the Oconee and Ocmulgee river basins. This type of study supports development of environmental flow regulations in the Oconee and Ocmulgee river basins and contributes to the improvement of local water management and planning. This will contribute to economic development of the region as a support of the UGA-Archway Partnership for the Ocmulgee River Water Trail National Park Initiative.

Introduction

Freshwater ecosystems, a foundational component of our human society, culture, and economy, are becoming increasingly compromised [1]. Humans currently capture more than 50% of available freshwater runoff and have fragmented rivers systems with upwards of 1,000,000 dams installed globally [2]. A wide range of human activities has led to rivers being deemed the earth's most damaged ecosystem, losing species at a greater rate than terrain and marine ecosystems [3]. It is imperative that rivers are managed in a more natural, sustainable way that balances the needs of both the aquatic ecosystems and the human livelihoods that rely on them. Environmental flow regimes are offered as at least a partial solution to some of the freshwater challenges that are currently in our midst. Previous research shows a relationship between flow and fish biomass based on a study of Austrian rivers [4].

According to the Middle Ocmulgee Regional Water Plan, the population in the region is projected to double by 2050 which will involve water demand increase by 38% and wastewater generation by 62% by 2050 [5]. Therefore, it is important to examine trade-offs in water management to support a sustainable ecosystem of the region. In Georgia, trade-offs study for water management strategies along the Oconee River has been conducted by S. K. McKay, 2014 [6]. In his study, S. K. McKay examined environmental flow and constructed a decision-making framework for the Middle Oconee River near Athens, Georgia [7].

Furthermore, C. A. Gibson et al., 2005 conducted a study of two river basins (Cle Elum River, Washington and Chattahoochee-Apalachicola River Basin, Georgia and Florida) to investigate the impact of future climate scenarios on river ecosystem. They demonstrated significant changes in flow regimes and aquatic habitat under various climate scenarios [8].

Additionally, a comparison study of two rivers in Northern Michigan (Carp Lake River and Little Black River) was conducted by J. Dillon to examine ecological effects of agricultural development on stream habitat and nutrient input [9]. In Alabama, Swinson (2014) studied the Tulotoma snail habitat along the Coosa River. The main focus of his study was contour generation using HEC-RAS software based on geo-referenced bathymetry of Coosa River [10]. Moreover, Yao and Georgakakos, 2001 introduced a concept of adaptive water resources management in their study of Folsom Lake, California. The adaptive system demonstrated reliable forecasts for better reservoir performance when compared to traditional one [11, 12]. Also, A. Chen et al., 2015 addressed trade-offs for better water management of Jordan River in the Middle East and Colorado River in the western United States [13]. They addressed similarities and differences of the two river basins by considering various factors, such as increasing water demand and supply and environmental flow demand.

Freeman et al., 1997 developed habitat suitability criteria for nine fish species by including depth, velocity, substrata type and cover [14]. For Eastern warm water US rivers, researchers suggest that it is not practical to collect habitat data due to a high number of the present species [15]. Therefore, researchers used more generalized criteria for habitat analysis rather than species-specific criteria [16].

Tuning of the input parameters is usually required to reduce the error between observed and predicted values. This process is often called as calibration in engineering field which is fundamentally equivalent to solving the inverse problem for deterministic computer simulator in statistics. We implement Gaussian process (GP) model which is a stochastic approximation of the output of deterministic computer simulator. GP model is very inexpensive when compared to evaluation of deterministic simulator [17]. R package GPfit uses a multi-start gradient-based search algorithm for likelihood optimization (using a maximum likelihood approach). Ranjan et al. (2008) proposed a novel expected improvement (EI) criterion for estimating a prespecified contour from an expensive deterministic simulator which gives scalar outputs [18]. They have further investigated this problem in Ranjan 2013, and Bingham et al. 2014 [19, 20].

Methods

We alter historical flow data for the river using a hydrologic model with a goal of relating changes in river discharge to changes in river depth and velocity, both of which are key criteria of habitat suitability. We then use generalized habitat suitability criteria to analyze how habitat distribution and degradation change with increasing water withdrawal rates. Additionally, we study how available habitat changes across a range of different flow regimes. Four scenarios of municipal water withdrawal and environmental flow requirements are simulated:

1. Unaltered: A reference condition without withdrawal defined the best attainable ecological condition and served as a point of relative comparison for other scenarios.
2. Annual minimum flow (AMF): This method assigns a single, year-round flow threshold below which water may not be withdrawn. The minimum flow threshold was varied from 0 to 1,000 cfs by 10 cfs increments to assess the influence of minimum flow magnitude on ecological conditions.

3. Monthly minimum flow (MMF): This method assigns a monthly-varied flow threshold below which water may not be withdrawn, which incorporates elements of flow timing not captured in annual minimum flows. Flow thresholds were varied in 101 intervals from the minimum observed monthly-averaged flow to the maximum observed monthly-averaged flow for the 60-year record for each of the 12 months.
4. Percent of flow (POF): This method withdraws a specified percentage of the unaltered discharge, which was varied from 0 to 50% by 0.5%.

We use R statistical software to simulate hydrologic alteration associated with different flow regime scenarios. We use the USACE Hydrologic Engineering Center’s River Analysis System (HEC-RAS) to model river hydraulics and create a set of hydraulic variables (mainly depth and velocity), which are often more ecologically relevant. We then calculate suitability for each habitat type using a Python script. Furthermore, we spatially visualize outputs of hydraulic and habitat models using ArcGIS®. A dynamic computer model is becoming very common and is one of the most popular sources of big data. For model calibration in case of complex dynamic physics models, we take Bayesian approach (history matching algorithm) to solve the inverse problem. This algorithm is Gaussian process based algorithm, and it is efficient especially when deterministic model runs/experiments are computationally or financially expensive. The inverse problem is often used for calibrating the computer model in the history matching context, modelling bias between the model and the true underlying physical process, and achieving the target process value.

Gaussian Process for solving inverse problem using History Matching Algorithm

Constructing emulator and solving the inverse problems help us to gain more insights into the system. Therefore, History Matching algorithm can be used to match the data points (observed) with the deterministic model to integrate the deterministic and probabilistic approaches. In this modeling approach, we implement Bayesian techniques to capture bias of a deterministic model. To consider the model uncertainty, we emulate, calibrate and validate the model using R package SAVE. SAVE package will help us to overcome challenges of computationally expensive models.

Figure 1 shows an illustrative example where the simulator $g(\cdot)$ takes an input $x = (x_1, x_2) \in [0,1]^2$ and generates a time-series response marked as gray dashed curves wherein the true field data given as a solid red curve. Figure 1 indicates the presence of a systematic shift (called bias) between the simulator runs and the field data. For this illustrative example, we used $g(x_0) + b_t(x)$ to obtain the field data. Our objective is to find $x \in [0,1]^2$ such that $g(x) \cong g(x_0)$.

We used a naive algorithm and history matching algorithm for solving this inverse problem and compare their performance. We found the common solution of the inverse problem for both algorithms to be very close to the true input values of $x_1 = 0.5$ and $x_2 = 0.5$. Figure 2 shows the comparison between solutions of the two methods. We can see the intersection of solutions 1, 2 and 3 to be close to the true values for both methods. Though the final solutions are similar in both methods, the total number of simulator evaluations are different (150 simulator runs for the naive approach vs. 71 simulator runs for history matching approach).

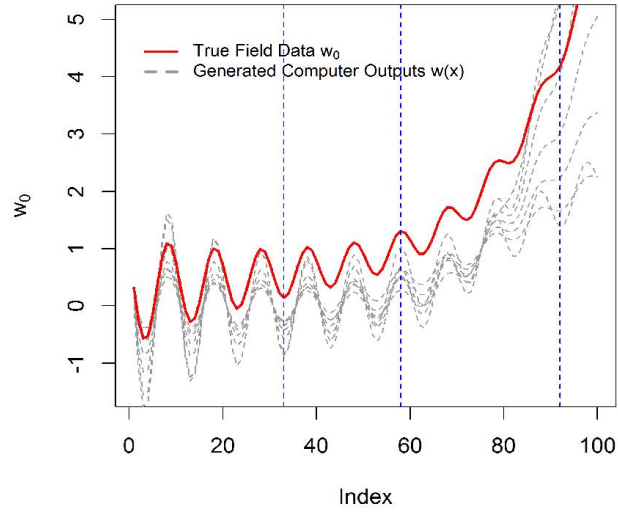


Figure 1. Simulated Computer Model Output

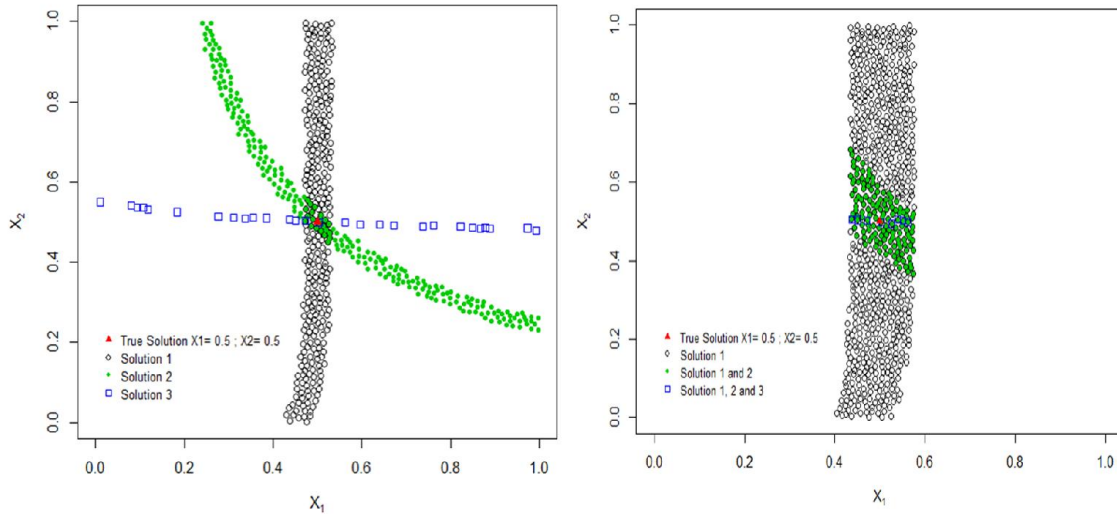


Figure 2. Inverse problem solution using naive approach (plot on the left) and history matching algorithm (plot on the right)

To include the bias term $b_t(x)$ introduced in Figure 1 and address the uncertainty of the model, we used R package SAVE developed by Palomo et al. (2015) [21]. Please note that we ran into error messages corresponding to the Cholesky Decomposition. To overcome this difficulty, we used the technique of data thinning. Thus, we divided the time range into 20 equal intervals and chose one point in each interval using Latin Hypercube sampling. *SAVE* function allowed us to construct the emulator using thinned data; *bayesfit* function was utilized to find estimates of the bias function; *validate* function was used to estimate the bias of the model. Figure 3 shows the original field data with the bias term, computer outputs, bias corrected prediction with uncertainty bounds and uncorrected prediction.

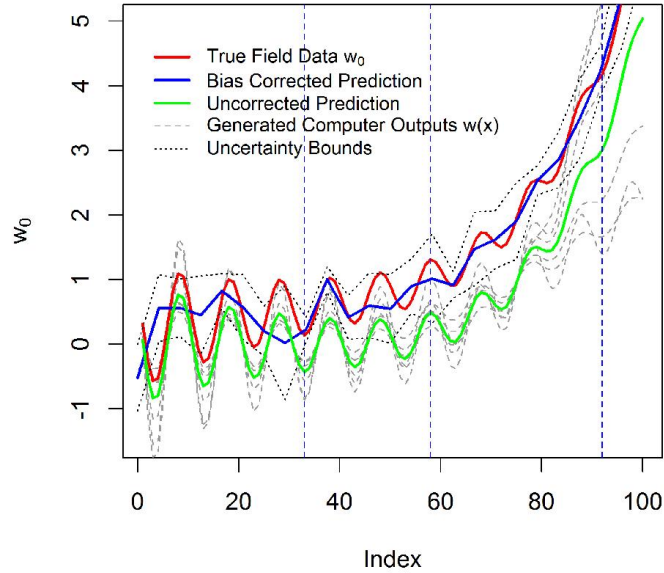


Figure 3. Illustrated example with the bias corrected prediction

Bathymetry Data Collection

To build an accurate hydrologic model of the Middle Oconee and the Middle Ocmulgee river, we collected extensive topographic and bathymetric data.

The Middle Ocmulgee River. To collect bathymetry cross-sectional data for the Middle Ocmulgee river reach, we used kayak-mounted sonar-based GPS mapping system (Figure 4). Detailed description of the system can be found in the study of Swinson 2012 [22]. With the obtained data, we created a triangulated irregular network (TIN) that closely resembles the main channel, bank slopes, and flood plain surface of our study reach.



Figure 4. Bathymetry data collection: (a) kayak-mounted sonar-based GPS Mapping system, (b) aerial view of cross-sectional bathymetry data

The Middle Oconee River. LiDAR data from the Athens-Clarke County Planning Department were retrieved from the Middle Oconee River and the surrounding banks and floodplain areas. A real-time kinematic (RTK) unit was utilized to set up control on the eastern bank of the river within Ben Burton Park. The total station was then placed within a sightline of the cross-sectional bathymetric points and on land topographic points to be collected near the upstream portion of the reach. A Carlson data logger was connected to the total station and used to perform a “resection” on the control points (Figure 5).



Figure 5. Bathymetry data collection at the study site near the Middle Oconee River

Hydraulic Modeling

While hydrologic alteration is a common surrogate for ecological integrity [6], habitat analyses require that hydrologic change be converted into hydraulic variables (e.g., velocity and depth), which are often more ecologically relevant. Here, the USACE Hydrologic Engineering Center’s River Analysis System (HEC-RAS version 4.1.0) is applied to assess channel hydraulics along with the accompanying HEC-GeoRAS (Version 10.1), which facilitates geospatially explicit analyses in ArcGIS® [23]. In addition to terrain, HEC-RAS requires user-inputs related to flow paths, channel roughness, and channel slope. Flow paths were demarcated using HEC-GeoRAS. Following standard convention, floodplain flow paths were estimated as the center of mass between the top of the bank and the extent of the floodplain (roughly 1/3 of the distance from the banks and 2/3 from the floodplain extent). Channel roughness (i.e., Manning’s n) was estimated through an iterative, pseudo-calibration process. Manning’s n was predicted from standard tabulated values for the channel and floodplain environments (i.e., Tables 5-5 and 5-6 in Chow 1959) [24].

This process resulted in four distinct values of Manning’s n: 0.065 for the open, moderately vegetated left floodplain, 0.070 for the more densely vegetated right floodplain, 0.025 for sandy portions of the channel, and 0.040 for rocky or “shoaly” portions of the channel. To estimate channel slope, thalweg measurements in each cross-section (i.e., the deepest point) were coupled with longitudinal distance downstream. These inputs provided a close representation of the pseudo-calibration observations. Figures 6 and 7 represent HEC-RAS models of the Middle Oconee and the Middle Ocmulgee Rivers, respectively.

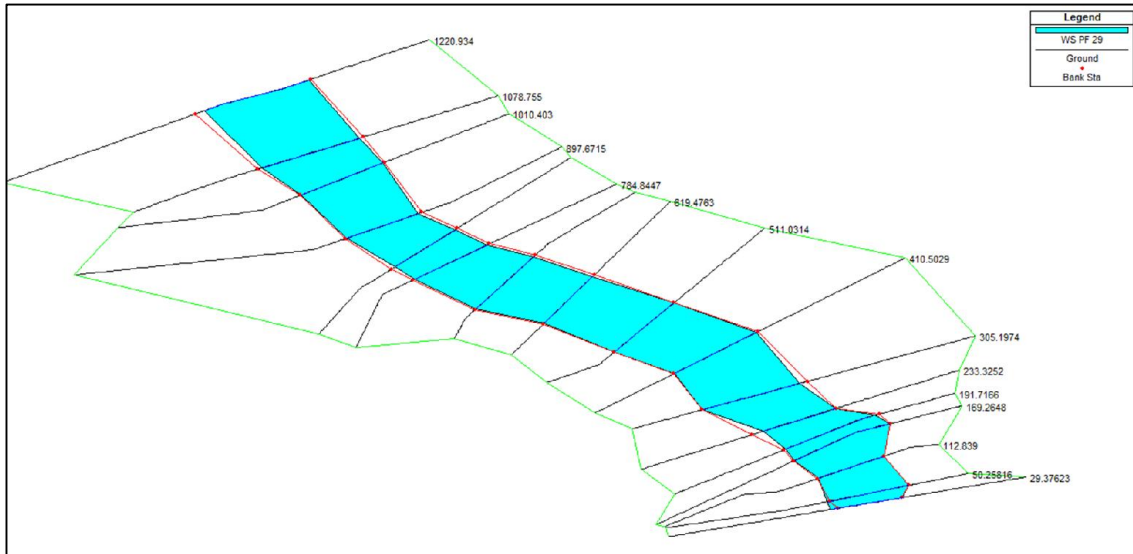


Figure 6. HEC-RAS Model for the Middle Oconee River.

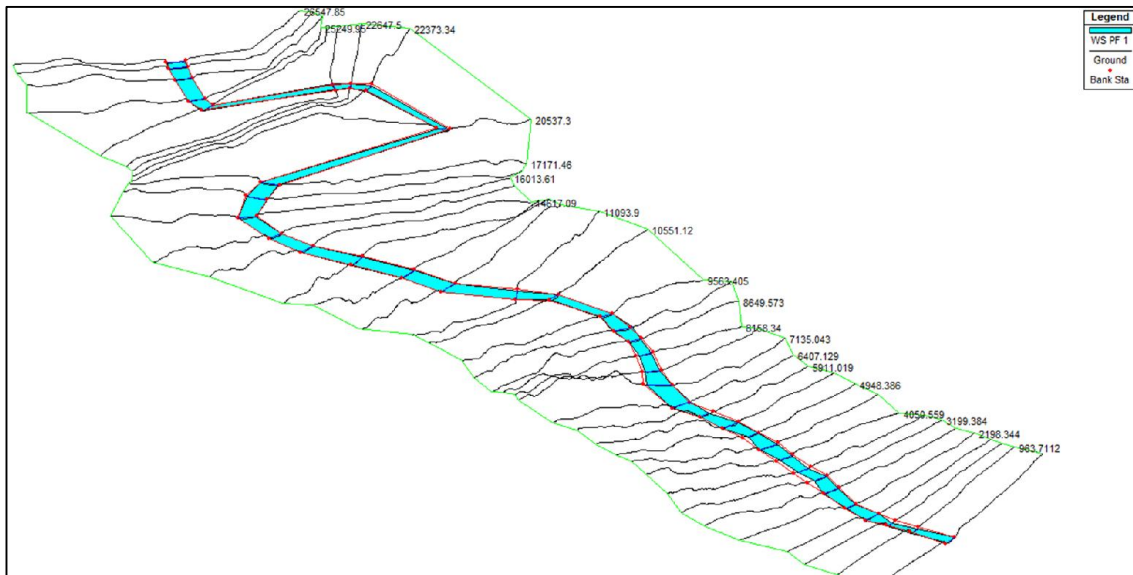


Figure 7. HEC-RAS Model for the Middle Ocmulgee River.

Suitability Habitat Model development

In our study, we included three types of the key habitat: shallow-fast, deep-fast and shallow-slow. Table 2 represents example taxa and suitability criteria in hydraulic terms such as river depth and flow velocity for each habitat type [16]. We analyzed different flow regimes and their impact on fish habitat by calculating the wetted usable area for each key habitat under each flow regime scenario.

Table 2. Habitat suitability criteria and representative taxa

Key Habitat	River Depth	Flow Velocity	Representative Taxa
1. Shallow – Fast	≤ 35 cm (≤ 1.15 ft)	≥ 55 cm/s (≥ 1.8 ft/s)	<i>Nocomis leptcephalus</i> (bluehead chub) <i>Notropis hudsonius</i> (spottail shiner)
2. Deep – Fast	≥ 35 cm (≥ 1.15 ft)	> 45 cm/s (> 1.48 ft/s)	<i>Micropterus Salmoides</i> (largemouth bass)
3. Shallow – Slow	< 35 cm (< 1.15 ft)	< 35 cm/s (< 1.15 ft/s)	<i>Lepomis</i> (bluegill and sunfish)

For each discharge, HEC-RAS was executed under steady-state conditions, and spatially explicit velocity and depth distributions were generated. A Python script was then applied in ArcGIS to calculate wetted usable area (i.e., total available habitat) and suitability for each habitat type for each of the discharge simulations (example for the Middle Oconee River shown in Figure 8).

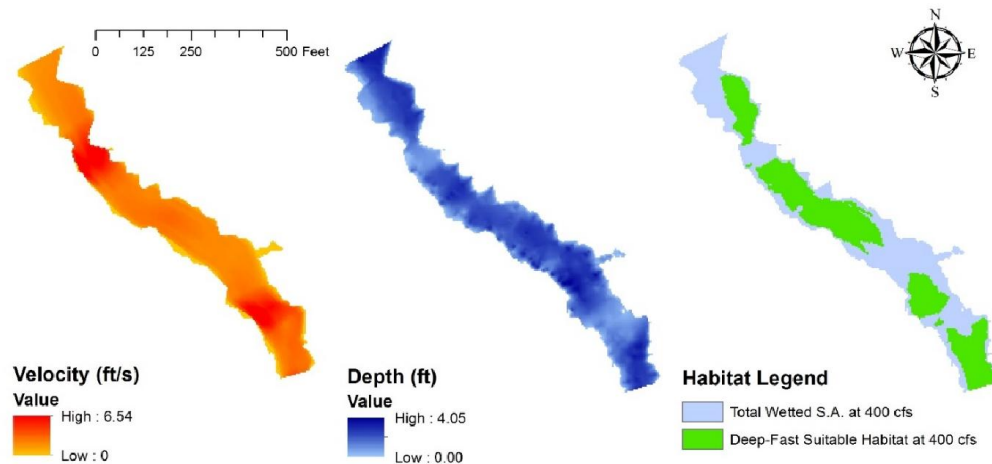


Figure 8. Example of spatially explicit outputs for hydraulic and habitat models for the Middle Oconee River at 400 cfs: (A) velocity, (B) depth, and (c) deep-fast habitat suitability.

Hydraulic and habitat simulations provided a mechanism to construct habitat rating curves for each of the four types of habitat assessed here (total, shallow-fast, deep-fast, and shallow-slow; Figure 9). As expected, total habitat increases with increasing discharge. However, the

distribution of habitat types changes dramatically over the range of discharges simulated.

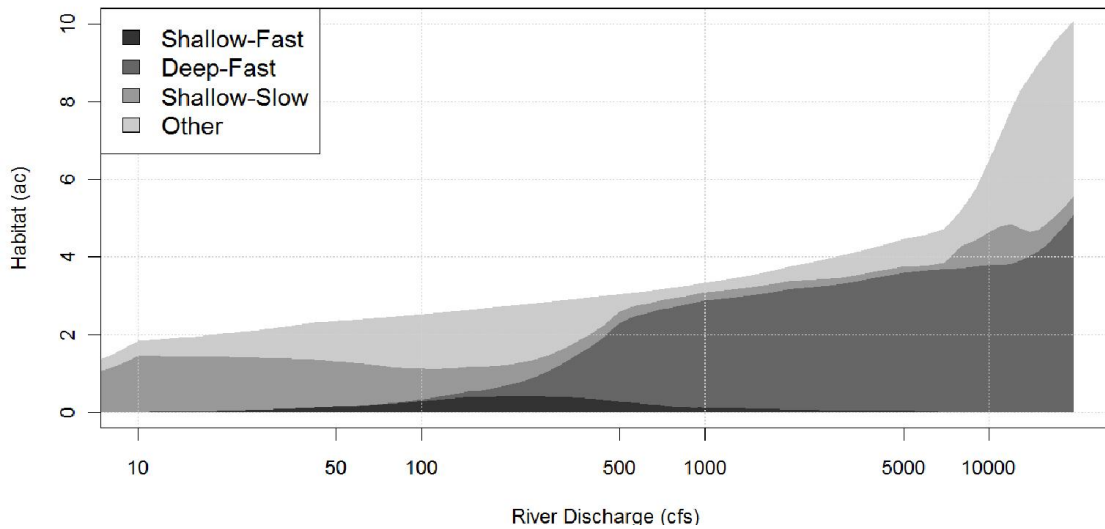


Figure 9. Cumulative habitat rating curves over the range of discharges observed in the Middle Oconee River.

Environmental Flow Alternatives

The simulations provide a mechanism to assess trade-offs between municipal water supply and habitat provision under the three environmental flow schemes (AMF, MMF, POF). The three environmental flow alternatives are compared on an equal withdrawal basis to find the most efficient alternative. Key differences emerge in the findings based on average annual discharge (Figure 10 top) or a magnitude-frequency analysis (Figure 10 bottom). First, total habitat is consistently over-predicted by the average discharge method. This is an expected outcome given that flow frequency distributions are often highly skewed, which leads to a mean discharge much greater than the median discharge (e.g., 521 cfs vs. 350 cfs for the Middle Oconee River). This skewed distribution is accounted for when incorporating the frequency of flows via effectiveness analysis, while average discharges can indicate a false sense of the quantity of habitat available. Second, only tracking average discharge can mask nuanced effects associated with alternative environmental flow regimes. For instance, the shallow-fast habitat assessments with magnitude-frequency analysis show a non-monotonic response, potentially due to changes in low flows as well as central tendencies. Third, the relative ranking of environmental flow alternatives shifts depending on whether average or frequency-weighted conditions are used.

To consider the impact of development on the environment, it is essential to study flow regimes and trade-offs involved in water management. Here, a new coupling of analytical techniques is presented, which helps incorporate natural variability into environmental flow studies. In doing so, we demonstrate the importance of hydrologic variability, not only relative to ecological outcomes, but relative to water management decision making.

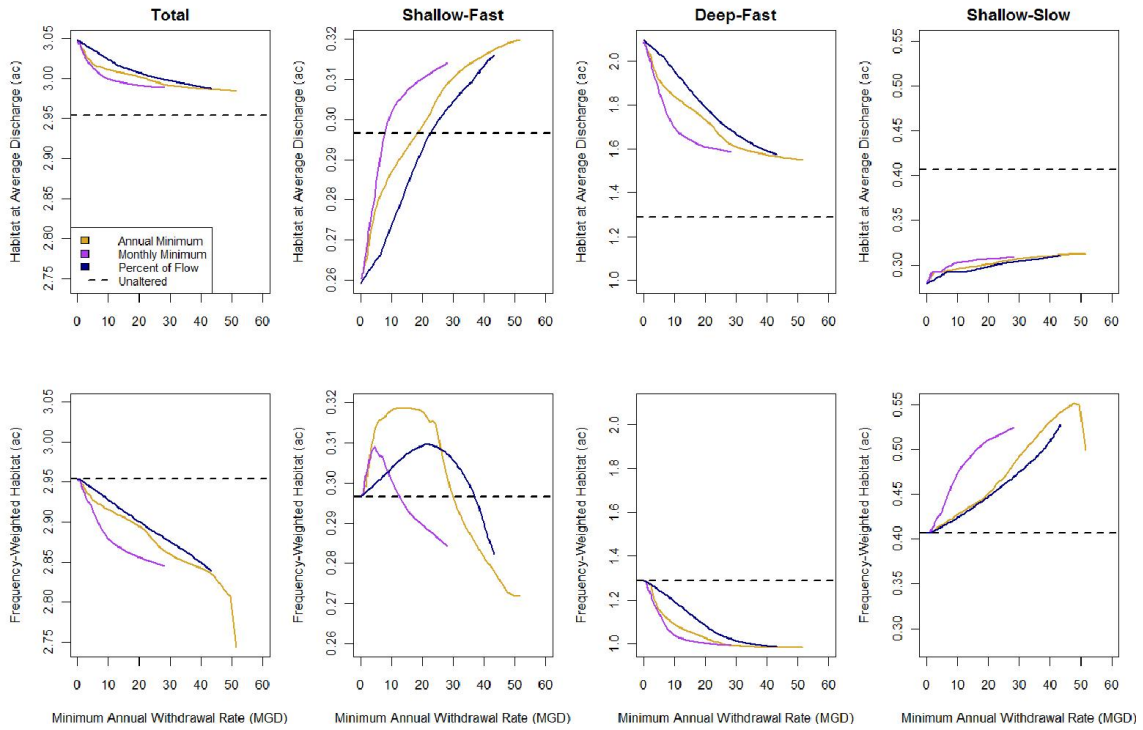


Figure 10. Comparison of environmental flow alternatives across total habitat and three distinct habitat types in the Middle Oconee River. (top) Habitat computed only at average discharge. (bottom) Habitat computed as a frequency-weighted quantity using effectiveness analysis.

Publications and Presentations

- **N. V. Bhattacharjee**, J. R. Willis, S. K. McKay and E. W. Tollner, "Habitat provision associated with environmental flows", *under review for USACE (U.S. Army Corps of Engineers) publication*.
- **N. V. Bhattacharjee**, P. Ranjan, A. Mandal and E. W. Tollner, "Inverse Modeling and Sensitivity Analysis for Rainfall-Runoff Computer Model using History Matching", *to be submitted to Journal of Environmental Management*.
- **N. V. Bhattacharjee**, J. R. Willis, K. W. Swinson and E.W. Tollner, "Water management and habitat suitability study along the Ocmulgee river", *17th Annual Meeting of the American Ecological Engineering Society (AEES), 23-25 May 2017, Athens, Georgia, USA*.
- **N. V. Bhattacharjee**, J. R. Willis, S. K. McKay and E.W. Tollner, "Habitat provision associated with environmental flows", *21st Century Watershed Technology Conference and Workshop, 3-9 December 2016, Quito, Ecuador*.
- **N. V. Bhattacharjee** and E.W. Tollner, "Improving management of windrow composting systems by modeling runoff water quality dynamics using recurrent neural network", *Ecological Modeling* 339 (2016): 68-76.
- **N. V. Shim**, E. W. Tollner, J. R. Willis and S. K. McKay, "Comparison of Oconee and Ocmulgee river basins for water management improvement", *2016 American Society of Agricultural and Biological Engineers (ASABE) Annual International Meeting, 17-20 July 2016, Orlando, Florida, USA*.
- **N. V. Shim** and E. W. Tollner, "Developing tools for modeling selected ecological changes induced by upstream reservoir management along a small river using HEC-RAS, HEC-EFM and additional spatial statistical tools", *2015 American Society of Agricultural and Biological Engineers (ASABE) Annual International Meeting, 26-29 July 2015, New Orleans, Louisiana, USA*.
- **N. Shim** and M. Elliott, "Ride it, Paddle it or Hike it: All Trails are Money Makers", *2015 Georgia Trail Summit, 4 - 6 June 2015, Athens, GA, USA*

References

1. Strayer, D.L. and D. Dudgeon, *Freshwater biodiversity conservation: recent progress and future challenges*. Journal of the North American Benthological Society, 2010. **29**(1): p. 344-358.
2. Jackson, R.B., et al., *Water in a changing world*. Ecological applications, 2001. **11**(4): p. 1027-1045.
3. Dudgeon, D., et al., *Freshwater biodiversity: importance, threats, status and conservation challenges*. Biological reviews, 2006. **81**(02): p. 163-182.
4. Moog, O., *Quantification of daily peak hydropower effects on aquatic fauna and management to minimize environmental impacts*. Regulated Rivers: Research & Management, 1993. **8**(1-2): p. 5-14.
5. *Middle Ocmulgee Regional Water Plan*. 2011.
6. McKay, S.K., *Quantifying Tradeoffs Associated with Hydrologic Environmental Flow Methods*. JAWRA Journal of the American Water Resources Association, 2015.
7. McKay, S.K., *Informing flow management decisions in the Middle Oconee River*. 2014.
8. Gibson, C., et al., *Flow regime alterations under changing climate in two river basins: implications for freshwater ecosystems*. River Research and Applications, 2005. **21**(8): p. 849-864.
9. Dillon, J. *Comparison of two rivers in Northern Michigan for determination of differential effects of development*. 2013; Available from: http://deepblue.lib.umich.edu/bitstream/handle/2027.42/101886/Dillon_Jeff_2013.PDF?sequence=1&isAllowed=y.
10. Swinson, K. *Contour Generation to Support Calculation of Exposed Snail Habitat in the Coosa River, Alabama*. in *American Water Resources Association Conference*. 3-6 November 2014. Tysons Corner, VA, USA.
11. Yao, H. and A. Georgakakos, *Assessment of Folsom Lake response to historical and potential future climate scenarios: 2. Reservoir management*. Journal of Hydrology, 2001. **249**(1): p. 176-196.
12. Georgakakos, A., et al., *Value of adaptive water resources management in Northern California under climatic variability and change: Reservoir management*. Journal of hydrology, 2012. **412**: p. 34-46.
13. Chen, A., et al., *A tale of two rivers: Pathways for improving water management in the Jordan and Colorado River basins*. Journal of Arid Environments, 2015. **112**: p. 109-123.
14. Freeman, M.C., Z.H. Bowen, and J.H. Crance, *Transferability of habitat suitability criteria for fishes in warmwater streams*. North American Journal of Fisheries Management, 1997. **17**(1): p. 20-31.
15. Bowen, Z.H., M.C. Freeman, and K.D. Bovee, *Evaluation of generalized habitat criteria for assessing impacts of altered flow regimes on warmwater fishes*. Transactions of the American Fisheries Society, 1998. **127**(3): p. 455-468.
16. Bain, M., *Habitat at the local scale: multivariate patterns for stream fishes*. Bulletin Francais de la Peche et de la Pisciculture (France), 1995.
17. Ranjan, P., R. Haynes, and R. Karsten, *A computationally stable approach to Gaussian process interpolation of deterministic computer simulation data*. Technometrics, 2011. **53**(4): p. 366-378.

18. Ranjan, P., D. Bingham, and G. Michailidis, *Sequential experiment design for contour estimation from complex computer codes*. Technometrics, 2008. **50**(4).
19. Ranjan, P., *Comment: EI criteria for noisy computer simulators*. Technometrics, 2013. **55**(1): p. 24-28.
20. Bingham, D., P. Ranjan, and W.J. Welch, *Design of computer experiments for optimization, estimation of function contours, and related objectives*. Statistics in Action: A Canadian Outlook, 2014. **109**.
21. Palomo, J., R. Paulo, and G. Garcia-Donato, *SAVE: an R package for the Statistical Analysis of Computer Models*. Journal of Statistical Software, 2015. **64**(13): p. 1-23.
22. Swinson, K.W., *Analysis of Georeferenced Sonar-Based Thalweg and Cross-Sectional River Depth Profile Measurements*. 2012.
23. Brunner, G.W., *HEC-RAS River Analysis System: User's Manual*. 2001: US Army Corps of Engineers, Institute for Water Resources, Hydrologic Engineering Center.
24. Chow, V., 1959, *Open channel hydraulics*, McGraw-Hill, New York.

Information Transfer Program Introduction

None.

USGS Summer Intern Program

None.

Student Support					
Category	Section 104 Base Grant	Section 104 NCGP Award	NIWR-USGS Internship	Supplemental Awards	Total
Undergraduate	4	0	0	0	4
Masters	1	0	0	0	1
Ph.D.	3	0	0	0	3
Post-Doc.	0	0	0	0	0
Total	8	0	0	0	8

Notable Awards and Achievements